AN s-WAVE I = 0 $\pi\pi$ RESONANCE

by

Bryan F. Gore

TECHNICAL REPORT NO. 71-012
August, 1970

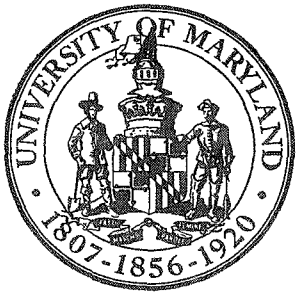

CENTER FOR THEORETICAL PHYSICS
OF THE
DEPARTMENT OF PHYSICS AND ASTRONOMY
UNIVERSITY OF MARYLAND
COLLEGE PARK, MARYLAND

AN s-WAVE I = 0 $\pi\pi$ RESONANCE*

by

Bryan F. Gore

Center for Theoretical Physics
Department of Physics and Astronomy
UNIVERSITY OF MARYLAND
College Park, Maryland

and

CENTRAL WASHINGTON STATE COLLEGE
Ellensburg, Washington 98926

TECHNICAL REPORT NO. 71-012

August, 1970

*Supported in part by the National Science Foundation under Grant NSF GY-5461. Computer time was furnished by the University of Maryland Computer Science Center under NASA Grant NsG-398.

ABSTRACT

Solutions are presented for subtracted dispersion relations, written for the s and p-wave inverse $\pi\pi$ scattering amplitudes with (CDD) poles inserted into both s-waves. These solutions predict the existence of a super broad I = 0 s-wave resonance (σ) accompanied by a small, negative I = 2 phase shift, in the absence of any s-wave experimental input whatsoever. While p-wave subtraction parameters are adjusted to fit a 755 MeV ρ resonance with width 120 MeV, the s-wave parameters are determined by crossing symmetry through derivative conditions to third order. The coupling constant, λ, is a free parameter, and resonant solutions are obtained for $-.033 \leq \lambda \leq .040$ with σ masses ranging from 550 to 900 MeV. In no case does δ_o^o rise to 135° by 1 BeV. On the basis of a sum rule, solutions with $\lambda > .007$ are preferred. The data from which two experimental analyses predicted the scattering length ratio $a_o/a_2 = -3$ are compared to predictions based on the solutions. Agreement is obtained for solutions with $.007 < \lambda < .03$ with $-2 < a_o/a_2 < 0$. The "best" solution, with $\lambda = .020$, predicts a σ of 750 MeV and an I = 2 s-wave phase shift of -18° at the ρ mass. Its scattering lengths are $\mu a_o = .040$, $\mu a_2 = -.088$ and $\mu^3 a_1 = .032$, and $\delta_o - \delta_2 = 53°$ at 500 MeV.

I. INTRODUCTION

Lovelace's analysis of backward πp scattering data using dispersion relations,[1] provided one of the earliest indications of the existence of an s-wave $I = 0$ $\pi\pi$ resonance, the σ. Consequently, it has been something of a disappointment that dispersion relation calculations of $\pi\pi$ scattering, incorporating the restrictive conditions of unitarity and crossing symmetry, have until now failed to predict the σ without the input of additional s-wave information. Nevertheless Morgan and Shaw,[2] assuming the existence of a σ, have calculated a range of s-wave scattering lengths which includes those predicted by Weinberg from PCAC considerations.[3] Also, Tryon[4] has produced a σ in calculations using Weinberg's scattering lengths as input. This present paper, however, reports a series of calculations of subtracted dispersion relations, written for the $\pi\pi$ inverse partial wave amplitudes, which culminates in the prediction of a broad σ resonance, a small negative $I = 2$ phase shift, and s-wave scattering lengths in good agreement with earlier predictions, in the absence of any s-wave input whatsoever.

The solutions reported herein are ordered by the Chew-Mandelstam coupling constant λ, which is a free parameter in the calculations. The mass of the predicted σ resonance increases with λ, from 550 MeV for $\lambda = -.033$ to 900 MeV for $\lambda = .040$, as does its width. Further weakening of the s-wave $I = 0$ attraction with increasing λ is evidenced by a transition solution (δ_0^0 small and negative below 700 MeV, small and positive above) for $\lambda = .100$ which links the resonant solutions to the repulsive s-wave dominant solutions previously reported for large

positive λ.[5-7] While solutions could not be obtained for $\lambda < -.033$, projecting an increasing attraction with decreasing λ indicates the probable establishment of a bound state for larger negative λ. This bound state has already been reported in results which failed to exhibit resonant behavior.[6,7] Thus, in addition to predicting the existence of a σ resonance, these solutions provide an understanding of the interaction as a function of λ which explains earlier results whose interpretation was previously unclear.

The innovations which lead to the striking success of these calculations are the insertion of (CDD) pole terms into the dispersion relations for both of the s-wave inverse amplitudes, and the evaluation of parameters using derivative conditions to third order from crossing symmetry. The insertion of the pole terms allows the possibility of zeros in both s-wave partial wave amplitudes. While such zeros have been predicted from PCAC considerations,[3,8] no conditions from current algebra are imposed in the calculations. In fact, since crossing symmetry requires the first derivatives of the s-wave inverse amplitudes to be proportional to λ^{-2} [Eqs. (19), (20)], it is obvious that for small $|\lambda|$ this condition cannot be satisfied by dispersion integrals unless further structure is built in. Thus, even the motivation for the introduction of the pole terms is contained within this formalism. Nevertheless, for the resonant solutions the positions of the zeros of the I = 0 and 2 s-wave amplitudes, plotted one against the other, lie on a straight line passing through the point predicted by PCAC.

The single third derivative equation used here was derived and used in a previous paper by the author,[9] henceforth referred to as I. It was then impossible to ascertain the usefulness of this equation because in I it was only possible to obtain solutions for $|\lambda| > .1$ (which differed little from earlier non-resonant, s-wave dominant solutions). Since this equation was of unknown utility, and is also difficult to apply, initially it was not used to evaluate parameters in the calculations reported here. However, it was found to provide an unambiguous choice among resonant solutions produced when the I = 2 s-wave phase shift was fixed at experimental values. Its subsequent imposition in determining parameters during iteration was the crucial step in obtaining the clear understanding of the interaction as a function of λ which has already been described.

II. FORMALISM

In terms of the variable $\nu = s/4 - 1$, where s is the center of mass energy squared (natural units, $m_\pi = 1$), the unitarity condition for elastic scattering is

$$A_\ell^I(\nu) = [(\nu+1)/\nu]^{1/2}(\cot \delta_\ell^I - i)^{-1} \quad , \tag{1}$$

where $\nu > 0$ and the phase shifts, δ_ℓ^I, are real. This relation is assumed valid within the energy range of these calculations. The once subtracted dispersion relations for the s-wave inverse amplitudes $F_I(\nu) = A_0^I(\nu)^{-1}$, with pole terms inserted, are

$$F_{I=0,2}(\nu) = \alpha_I + \beta_I/(1-\gamma_I\nu) + f(\nu) + L_I(\nu) - i\,\mathcal{I}_I(\nu) \tag{2}$$

and the twice subtracted p-wave dispersion relation, written for $F_1(\nu) = \nu A_1^1(\nu)^{-1}$ is

$$F_1(\nu) = \alpha_1 + \beta_1\nu + \nu f(\nu) + L_1(\nu) - i\nu\,\mathcal{I}_1(\nu) \quad . \tag{3}$$

($F_1(\nu)$ lacks the threshold singularity of $A_1^1(\nu)^{-1}$.) The integral over the right hand cut discontinuity (given by unitarity) is

$$\begin{aligned} f(\nu) &= -\frac{\nu}{\pi} P \int_0^\infty \frac{[\nu'/(\nu'+1)]^{1/2}}{\nu'(\nu'-\nu)}\, d\nu' \\ &= \frac{2}{\pi}\left(\frac{\nu}{\nu+1}\right)^{1/2} \ln\left(\sqrt{|\nu+1|}+\sqrt{|\nu|}\right) \\ &\qquad\qquad \text{for } \nu > 0 \text{ or } \nu < -1 \\ &= \frac{2}{\pi}\left(\frac{-\nu}{1+\nu}\right)^{1/2} \tan^{-1}\left(\frac{1+\nu}{-\nu}\right)^{1/2} \\ &\qquad\qquad \text{for } -1 < \nu < 0 \quad . \end{aligned} \tag{4}$$

The integral over the left hand cut discontinuity is

$$L_I(\nu) = -\frac{\nu^{\ell+1}}{\pi} P \int_{-\infty}^{-1} \frac{\text{Im } A_\ell^I(\nu')d\nu'}{\nu'^{\ell}(\nu'-\nu)|A_\ell^I(\nu')|^2} \quad , \tag{5}$$

and the imaginary parts of the inverse amplitudes are

$$\mathcal{J}_I(\nu) = \left(\frac{\nu}{\nu+1}\right)^{1/2} \theta(\nu) + \frac{\text{Im } A_\ell^I(\nu)}{|A_\ell^I(\nu)|^2} \theta(-\nu-1) \quad . \tag{6}$$

Using approximate crossing symmetry, the left hand cut discontinuity is expressed in terms of the right hand cut discontinuity in the crossed channels;

$$\text{Im } A_\ell^I(\nu) = \frac{2}{\nu} \int_0^{-\nu-1} d\nu' \, P_\ell \left(1 + 2\,\frac{\nu'+1}{\nu}\right) \times \sum_{I'} \chi_{II'} \sum_{\ell'} (2\ell'+1) P_{\ell'}\left(1 + 2\,\frac{\nu+1}{\nu'}\right) \text{Im } A_{\ell'}^{I'}(\nu') \quad , \tag{7}$$

where χ is the usual crossing matrix

$$\chi = \begin{pmatrix} 1/3 & 1 & 5/3 \\ 1/3 & 1/2 & -5/6 \\ 1/3 & -1/2 & 1/6 \end{pmatrix} \quad , \tag{8}$$

and the partial wave expansion is truncated after p-waves. On the right hand cut Im $A_\ell^I(\nu)$ may be written using the unitarity condition as soon as Re$[A_\ell^I(\nu)^{-1}]$ is known. Hence iteration proceeds by neglecting $L_I(\nu)$ and evaluating parameters, then computing $L_I(\nu)$, recomputing parameters, etc., until all parameters change by less than one per cent in the last iterative loop.

The eight parameters introduced by pole terms and subtractions are evaluated by a combination of conditions from crossing symmetry and experiment. The p-wave subtraction constants are fixed by the mass and width of the ρ resonance by requiring

$$\left(\frac{\nu^3}{\nu+1}\right)^{1/2} \cot\delta_1^1 \Big|_{\nu_\rho} = 0 \tag{9}$$

and

$$\frac{d}{d\nu}\left[\left(\frac{\nu^3}{\nu+1}\right)^{1/2} \cot\delta_1^1\right]_{\nu_\rho} = -\frac{1}{\gamma}\left(\frac{\nu_\rho^3}{\nu_\rho+1}\right)^{1/2} \tag{10}$$

with $\nu_\rho = 6.25$ and $\gamma = 1.15$, corresponding to a resonance of mass 755 MeV and width 120 MeV. Thus, at the ρ resonance the p wave has the same slope as if it were given by the Breit-Wigner form

$$A_1^1(\nu) = \left(\frac{\nu+1}{\nu}\right)^{1/2} \frac{\gamma}{\nu_\rho - \nu - i\gamma} \quad . \tag{11}$$

Crossing symmetry, applied at the symmetry point of the Mandelstam triangle, provides derivative conditions which may be used to evaluate parameters. Although an infinite number of conditions are available, higher partial waves become more important in higher derivative conditions. Consequently, in the following derivative conditions (Eqs. (21), (22a), (22b), (26) and (28) of I), d-waves have been removed from the second derivative condition, and both d and f-waves have been removed from the third derivative condition, by parameterizing them near threshold and combining equations:

$$2A_0^0 = 5A_0^2 \quad , \tag{12}$$

$$\frac{dA_0^0}{d\nu} = -2\,\frac{dA_0^2}{d\nu} \tag{13}$$

$$= -9\,A_1^1 \quad , \tag{14}$$

$$\frac{d^2A_0^0}{d\nu^2} - \frac{5}{2}\,\frac{d^2A_0^2}{d\nu^2} = 27A_1^1 + 18\,\frac{dA_1^1}{d\nu} \quad . \tag{15}$$

$$-\frac{1}{3}\left(\frac{d^3A_0^0}{d\nu^3} - \frac{5}{2}\,\frac{d^3A_0^2}{d\nu^3}\right)$$

$$= \frac{675}{8}\,A_1^1 + \frac{225}{4}\,\frac{dA_1^1}{d\nu} + \frac{75}{4}\,\frac{d^2A_1^1}{d\nu^2} \quad . \tag{16}$$

These conditions are to be evaluated at the symmetry point $\nu_{sp} = -\frac{2}{3}$, and it is to be recalled that $A_0^0(\nu_{sp}) = -5\lambda$. Thus, with λ specified a priori as a free parameter, the six s-wave parameters may be evaluated without using conditions based upon experimental results.

Before discussing the application of these conditions it is perhaps in order to comment upon their usefulness. In Ref. 4, Tryon comments that when d-waves are kept, the solutions of partial wave dispersion relations satisfy second and all higher derivative conditions identically; thus they are not useful to him in determining parameters. Within the formalism used here, unless the pole term parameters are chosen to satisfy a given condition there is clearly no reason to expect it to be satisfied. Thus the usefulness of a condition must be determined by whether or not it provides a means of discriminating between possible choices of a parameter, or solution. The usefulness of the third derivative equation [Eq. (16)] was seriously questioned when early calculations showed it to be well satisfied over a wide range of λ by solutions obtained when

δ_0^0 was required to resonate at 745 MeV. However, when the resonance condition was replaced by one fixing δ_0^2 there, Eq. (16) provided an unambiguous means of discriminating between the solutions. With its utility thus established it was then successfully used to replace the condition from experiment in determining parameters.

Although it may not be immediately obvious, the application of the derivative equations to determine parameters is straightforward. First the conditions are expressed in terms of the inverse functions F_I. With λ specified a priori, the zeroth and first order equations provide four conditions, each linear in only one of the s-wave functions $F_{0,2}$ (recall that the p-wave is completely known from the ρ mass and width):

$$\lambda = -(5F_0)^{-1} \tag{17}$$

$$= -(2F_2)^{-1} \tag{18}$$

$$\frac{dF_0}{d\nu} = -6(25\lambda^2 F_1)^{-1} \tag{19}$$

$$\frac{dF_2}{d\nu} = 3(4\lambda^2 F_1)^{-1} \tag{20}$$

While differentiation of the numerically evaluated left cut integrals is difficult after integration, Eq. (5) may be differentiated any number of times prior to the integration. Since the resulting integrals converge even more rapidly, no accuracy is lost by this procedure.

The second and third derivative conditions are slightly more complicated to apply because they involve both s-waves. Nevertheless, when a condition from experiment is applied to either one of the s-waves, that condition plus

two of the above conditions allow the evaluation of the three parameters of that partial wave via linear equations. With one s-wave known, the second derivative condition (incorporating Eqs. (17)-(20)),

$$\frac{d^2F_0}{d\nu^2} - \frac{2}{5}\frac{d^2F_2}{d\nu^2} = -(5\lambda F_1)^{-2}(12\frac{dF_1}{d\nu} - \frac{81}{10\lambda}) \tag{21}$$

may be linearly combined with the other two equations above, specifying all parameters unambiguously. The third derivative equation (expressed incorporating Eqs. (17)-(20)),

$$\frac{d^3F_0}{d\nu^3} - \frac{2}{5}\frac{d^3F_2}{d\nu^3} - \frac{18}{5\lambda F_1}(2\frac{d^2F_0}{d\nu^2} + \frac{d^2F_2}{d\nu^2}) - \frac{7F_1^{-3}}{12}(\frac{9}{5\lambda})^4$$

$$= 3(\lambda F_1)^{-2}[(\frac{1}{2}\frac{d^2F_1}{d\nu^2} - \frac{1}{F_1}(\frac{dF_1}{d\nu})^2] \tag{22}$$

may then be evaluated straightforwardly.

When Eq. (22) is used in solving for parameters, a quadratic equation results for the ratio γ_I/β_I for one of the s-waves. Consequently, two sets of parameters are produced. In general, initially choosing the set with $\alpha_o < 0$, then minimizing the change in γ_o resulted in solutions, while the opposite initial choice led to imaginary roots. However, for $\lambda < -.008$ the initial roots were imaginary. This difficulty was overcome by assuming initial values for the $L_I(\nu)$ and their derivatives at the symmetry point taken from solutions obtained for the same λ values when the resonance was required. Even this technique failed for $\lambda < -.033$, when after a few iterations the roots became imaginary.

III. RESULTS

Calculations were carried out for three cases. In the first, δ_0^0 was required to resonate at 745 MeV; in the second, δ_0^2 was fixed within its experimentally determined range near the ρ mass; in the third case the third derivative condition was imposed. In all cases λ was fixed a priori as a free parameter, and solutions were obtained over as wide a range of λ as possible. Crossing conditions through the second derivative were enforced in all cases.

A. RESONANCE REQUIRED

The s-wave phase shifts of typical solutions obtained when a σ of 745 MeV[10] was required are shown in Fig. 1, and the related scattering lengths in Fig. 2. For $-.05 < \lambda < .05$, the scattering lengths agree within 5% with those computed by Morgan and Shaw[2] for a σ of 765 MeV. Thus, the general agreement found between their phase shifts and those of Fig. 1 is expected. Since the solutions presented here cover a wider range of λ, it is to be expected that as λ increases to .100 the sign change of δ_0^0 occurs at higher energy, and that as λ decreases to $-.080$, δ_0^0 increases more rapidly near threshold, than occurred in their limiting cases. Although they published no turnover δ_0^2 solutions, it may be assumed that they obtained them, since they obtained positive I = 2 scattering lengths for $\lambda < -.03$. A notable difference, however, is seen when the δ_0^0 curves of Fig. 1 are compared with those of Morgan and Shaw near the σ resonance. Their solutions, obtained by treating the width of the σ as an input parameter, exhibit a wide range of widths, while the formalism used here predicts only very broad, asymmetric resonances. Their weaker

conclusion that solutions with broad σ's are preferable is an indication of the greater power of the method used here.

Since all resonant solutions reported in this paper are very broad, it should be emphasized that this is a consequence of the crossing conditions employed, and cannot be attributed to inflexibility of the s-wave parametrization. To see this, note that as ν increases above the position of the pole of F_0^0 (lying either above or below threshold), $F_0^0(\nu)$ decreases from $+\infty$ to zero at the resonance. A continued decrease to -1, clearly allowed by the form of the parametrization, would correspond to δ_0^0 increasing to 135°. The absence of such an increase must therefore be attributed to the conditions used to fix the parameters, i.e. crossing symmetry.

The most surprising results of the calculations performed with the σ resonance required are shown in Fig. 3, where the right and left hand sides of Eq. (16), the third derivative equation, are plotted. This equation is seen to be surprisingly well satisfied over almost the entire range of λ shown, and clearly cannot be used to choose any one solution as best. When this was discovered, it was assumed that it was somehow due to the satisfaction of the lower derivative crossing conditions, and that the third derivative condition was therefore empty. It certainly seemed unlikely that the imposition of this condition would prove to be the critical step in obtaining resonant solutions over a wide range of λ (see section C).

With the loss of the third derivative condition as a means of discriminating between solutions, the possibility of firmly predicting the existence of a σ in this case vanished. Nevertheless, the progression of δ_0^2 with λ indicated the possibility of a δ_0^0 progression if δ_0^2 was constrained. This provided the motivation for the next set of calculations.

B. δ_0^2 FIXED NEAR THE ρ

Figs. 4-7 show the s-wave phase shifts of typical solutions obtained when the value of δ_0^2 at 745 MeV[10] was fixed in its experimentally determined range. The reproducibility of results within this formalism may be seen as follows: from Fig. 1, a σ near the ρ mass is predicted for $\lambda \gtrsim .04$ when $\delta_0^2 = -20°$; it is seen in Fig. 4 for $\lambda = -.038$. A similar σ may be expected for $\lambda \gtrsim 0$ when $\delta_0^2 = -15°$, and is seen in Fig. 5 for $\lambda = -.002$. The incompatibility, seen in Fig. 1, of a σ near the ρ mass and $\delta_0^2 = -10°$ is evident in the lack of such a solution in Fig. 6. Finally, for $\delta_0^2 = -20°$ a σ near the ρ mass is predicted for $\lambda \gtrsim -.06$ from Fig. 1. Although such a result was not obtained, a solution for $\lambda = -.057$, resonant at 1 BeV, is seen in Fig. 7. Thus the formalism is satisfactorily self-consistent.

The most obvious feature of Figs. 4-6, the decrease of the mass and width of the σ with increasing λ, turns out to be a misleading consequence of the constraint of δ_0^2. The decrease would seem to imply an attractive interaction, increasing in strength with λ. However, the solution for $\lambda = .057$ of Fig. 5 shows that instead of a bound state being formed for large λ (i.e. the resonance approaching, then going below threshold with

increasing λ) the interaction becomes repulsive. (Since intermediate solutions of this type most often failed to converge upon iteration, this conclusion was first reached by noting that the scattering lengths of Fig. 8 did not exhibit the discontinuity which would have corresponded to the establishment of a bound state.) The pertinant feature of these solutions is instead, the advance with increasing λ, of the pole of F_0^0 (zero δ_0^0) toward $\nu = \infty$ and its reappearance of large negative values of ν.

The true increase of attraction occurs with negative λ, culminating in the formation of the bound state seen in Fig. 7 for $\lambda = -.67$. However, only extremely heavy, broad σ's are produced here, with the lightest occurring at 1 BeV for $\lambda = -.057$. The close similarity of the solutions with $\lambda < -.13$ to the negative λ solutions obtained in I is probably due to the constraint of the I = 2 s-wave imposed in I by the insertion of a pole term into only the I = 0 s-wave.

In Fig. 8 the s-wave scattering lengths are plotted one against the other. The curves are from Morgan and Shaw, with the upper, middle and lower curves representing σ's of 900, 765 and 600 MeV respectively. The curve of Fig. 2, drawn for a σ of 745 MeV, would lie just slightly below the middle curve, as is expected. The progression of the points across the curves as the σ is established and moves toward threshold is in accordance with the ordering of the curves.

Order was introduced into this confusing welter of solutions by the resurrection of the third derivative condition. Eq. (16), applied to the various solutions, is shown in Fig. 9. It clearly selects a single solution

from each set computed for a given δ_0^2 value. For δ_0^2 values of -10°, -15° and -20° the preferred solutions have λ values of -.017, .007 and .038, and exhibit σ resonances with masses of 600, 660, and 750 MeV. Thus, with increasing λ the σ moves away from threshold, indicating a weakening attraction. The connection of these selected solutions with the repulsive solutions found in I for large positive λ is seen by the onset of repulsion indicated by the emergence of the pole of $F_0^0(\nu)$ (zero of δ_0^0) above threshold in the solution for $\delta_0^2 = -20$ with $\lambda = .038$.

Thus, the third derivative condition proved to be the condition which forces the existence of a σ resonance over a wide range of λ. Further, the interpretation of the solutions satisfying it is consistent with the previously existing information about the interaction as a function of λ. With its usefulness thus proven, the logical next step was to use it to obtain solutions completely devoid of s-wave input from experiment.

C. THIRD DERIVATIVE CONDITION IMPOSED

The s-wave phase shifts for typical solutions obtained when all s-wave parameters were fixed solely by conditions from crossing symmetry are shown in Fig. 10. The attraction causing the resonant δ_0^0's clearly weakens with increasing λ, and the solution with $\lambda = .100$ indicates the transition to the repulsive solutions previously obtained for $\lambda > .1$. The scattering lengths for these solutions agree closely with those computed when the resonance was required, and are plotted in Fig. 11. Imaginary roots obtained in solving for parameters prevented solutions with $\lambda < -.033$ or $\lambda > .1$.

The asymmetry of the δ_0^0 curves plus the fact that none of them rise above 135° by 1 BeV, makes it difficult, if not meaningless, to assign widths to the σ's indicated by the various curves. A common approximation is to quote the width of a Breit-Wigner resonance, the real part of whose inverse amplitude at the resonance position has the same slope (as in Eqs. (9)-(11)). For the solutions with $\lambda = -.033$, .007 and .040, above the resonance the square of such an amplitude falls to half of its maximum value at 710, 1050 and 2350 MeV. However, the corresponding point below the resonance lies below threshold for all solutions except that for $\lambda = -.033$, for which it lies at 310 MeV.

The locations of the zeros of the s-wave amplitudes are plotted one against the other in Fig. 12. For the resonant solutions, they lie on a straight line passing through the point predicted from PCAC considerations, which coincides with the solution with $\lambda = -.008$. Since the resonant solutions obtained for the other cases exhibited zeros lying on this same line, it was felt that this must be due to some invariant feature of the formulation. The most obvious possibility was a combination of the lowest order crossing conditions. Parametrizing the s-waves by

$$A_0^I(\nu) = a_I + b_I\nu \quad , \tag{23}$$

and applying only Eqs. (12) and (13) yielded the prediction

$$\nu_2 = -.8\nu_0 - 1.2 \tag{24}$$

for comparison with the line of Fig. 12,

$$\nu_2 = .740\nu_0 - 1.17 \quad . \tag{25}$$

Since the amplitudes are not linear, this is quite satisfactory agreement. The difference in slopes is mainly due to a systematic decrease, with increasing λ, of the second derivative of A_0^0 at the symmetry point.

In achieving the above prediction, it was seen that with only the additional imposition of condition (14) the scattering lengths would be related by

$$2a_0 - 5a_2 = 18/F_1^1(sp) \tag{26}$$

(still assuming linear s-waves). The Breit-Wigner ρ used to fix the p-wave in Eqs. (9) and (10) corresponds to $F_1^1(sp) = 31.9$, so the scattering lengths would lie on the line

$$a_2 = .4a_0 - .113 \quad . \tag{27}$$

Now in the actual calculations, the p-wave differs from a B-W resonance due to the cut integrals. Examination of the solutions shows that $F_1^1(sp)$ increases with λ, and agrees with the B-W value for $\lambda \gtrsim 0$ (Table I). For each solution it is straightforward to predict a line similar to Eq. (27), and (using the value of λ also) the point on the line expected if the s-wave amplitudes were linear. These predictions are shown in Fig. 11. From the surprising accuracy of these crude predictions it is clear that the scattering length curve is determined primarily by the lowest order crossing conditions and the p-wave at the symmetry point.

IV. PREFERRED SOLUTIONS

All of the resonant solutions of Fig. 10 are acceptable in the sense that their phase shifts near the ρ resonance lie within the range of values reported experimentally. Nevertheless, they differ significantly near threshold, with extreme solutions exhibiting a "turnover" phase shift in one or the other of the isospin states. Although phase shift analyses based on the scattering of charged pions are unreliable at low energies, and multi-valued as well, other experimental evidence exists which may be used to select a preferred solution on the basis of its low energy behavior. However, since so much has been achieved without recourse to experimental results, it is of interest first to see if theory can predict a "best" solution for comparison with the results of experiment.

Olsson[11] has recently noted that the shape of the scattering length curve may be qualitatively predicted, assuming a σ exists, by the use of the sum rule

$$2a_o - 5a_2 = 6L \tag{28}$$

where

$$L = \frac{1}{\pi}\int_0^\infty \frac{d\nu}{\nu(\nu+1)}\,\mathrm{Im}\left[\frac{1}{3}A^0 + \frac{1}{2}A^1 - \frac{5}{6}A^2\right] . \tag{29}$$

With the shape of the curve understood, however, it seems more pertinent to use this relation as a consistency check, asking whether or not the line predicted by Eq. (28) for a given solution passes through the point on the scattering length curve corresponding to that solution. Unfortunately, the convergence of the integral is slow, so that contributions from above 1 BeV are significant. The onset of inelasticity makes the amplitudes computed here unreliable above 1 BeV; fortunately, contributions

from the two s-waves and the p-wave almost cancelled in this region. Additional high energy contributions to L have been estimated by Tryon[4] as follows: from the $f_0(1250)$, .007; from the g(1650), .002; net "daughters" contribution from lower spin resonances beneath the f_0 and the g, .010; "Regge" contribution due to ρ exchange above 1.8 BeV, .013. Adding these contributions (totalling .032) to the contributions of the I = 0 and 2 s-waves and the p-wave (summed to 1.1 BeV) yields

$\lambda = -.033$:

$$L = .090 - .003 + .037 + .032 = .156$$

$\lambda = .007$:

$$L = .057 - .008 + .037 + .032 = .118 \qquad (30)$$

$\lambda = .040$:

$$L = .032 - .020 + .037 + .032 = .081$$

to which is appended Tryon's error estimate of $\pm$ .015 due to contributions from above 1 BeV.

In Fig. 13 the scattering length curve is re-drawn for comparison with the lines predicted by Eq. (28). Solutions with larger λ values and higher mass σ's are clearly more self-consistent than those with smaller λ values and lower mass σ's. The solution with $\lambda = .040$, whose point lies close to the .040 line, is very self-consistent, whereas the solution with $\lambda = .007$, whose point lies slightly outside the error bars for the .007 line, is consistent with one standard deviation from the prediction. Consequently, solutions with $\lambda > .007$ are preferred.

V. COMPARISON WITH EXPERIMENT

We now turn to the results of experiment. The analysis by Deinet et al.[12] of the reaction $\pi^- p \to \pi^o \pi^o n$ provides the best recent evidence for the existence of a σ. They find a cross section for $\pi^+\pi^- \to \pi^o\pi^o$ scattering consistent with the saturation of unitarity from 600 to 900 MeV. Their results are shown in Fig. 14 along with the cross section curves calculated from the solutions of Fig. 10. While the solution with $\lambda = -.033$ peaks and then falls at too low an energy, the rest of the solutions are consistent with the data. Thus the great widths of the predicted σ's are in agreement with experimental results above the mass of the ρ.

Two recent theoretical/experimental analyses[13,14] have predicted/deduced that the ratio of the s-wave scattering lengths is $a_0/a_2 = -3$, which would correspond to a solution with $\lambda \gtrsim 0$ in Fig. 13. However, when the predictions of the solutions of Fig. 10 are compared with the data, agreement is obtained in the range $.007 < \lambda < .03$, with $-2 < a_0/a_2 < 0$. This discrepancy is, of course, due to the approximations used in obtaining predictions from the data.

In the analysis of Cline, Braun and Scherer[13] the ratios of $\sigma(\pi^+\pi^- \to \pi^o\pi^o)$ to $\sigma(\pi^+\pi^- \to \pi^+\pi^-)$ and $\sigma(\pi^+\pi^+ \to \pi^+\pi^+)$ are shown to depend simply on $r = \sin\delta_0^0/\sin\delta_0^2 \gtrsim \delta_0^0/\delta_0^2$ near threshold. These ratios are averaged between 300 and 400 MeV (despite a fourfold variation in the former) and used to predict an average value for r which is assumed to equal a_0/a_2. In Figs. 15 and 16 the cross section ratios from their paper are shown along with the predictions of the solutions of Fig. 10. In both cases the low energy results are bracketed by the solutions with

λ = .020 and .007, with the former solution preferred by the 00/+- ratio and the latter by the 00/++ ratio.

In the analysis of Gutay, Meiere and Scharenguivel,[14] the helicity amplitudes for the reaction $\pi^- p \to \pi^+ \pi^- n$ are assumed to contain the factors $T_\ell^{+-}(s,\Delta^2)$, which are the off mass shell $\pi^+\pi^-$ partial wave scattering amplitudes, with $-\Delta^2$ the mass of the off-shell pion. T_0^{+-} is expressed in terms of linear, crossing-symmetric I = 0 and 2 s-wave amplitudes, constructed to satisfy the Adler consistency condition. (So constructed each amplitude is a function of the same two parameters, B and C, and the variables s and Δ^2.) Requiring T_0^{+-} to vanish yields a linear relation between Δ^2 and s (in terms of B and C) whose slope may be used to evaluate the ratio of the parameters, and consequently the ratio a_0/a_2. This slope is then evaluated from a plot of Δ^2 vs s for the zeros of the asymmetry of the $\pi\pi$ angular distribution (which occur when T_0^{+-} vanishes.) The obvious approximation to question here is the assumption of linear amplitudes above threshold.

Since the amplitudes for the solutions of Fig. 10 are not linear, a reasonable way of comparing them to the data is to fit a straight line to their values at the symmetry point, and at 400 MeV (fit to Re A_0^I above threshold). For this procedure the amplitudes are written

$$T_0^0 = -2\,B_0(s+2\Delta^2-1) + C_0(2s-\Delta^2-2)$$

$$T_0^2 = B_2(s-\Delta^2-1) - C_2(s+\Delta^2-1) \qquad (31)$$

which, with $B_0 = B_2$ and $C_0 = C_2$, agrees with Eq. (4) of Ref. 14 after

imposition of the Adler condition. The fourth pion is then put on the mass shell ($\Delta^2 = -1$), and the B's and C's evaluated by fitting to the symmetry point and 400 MeV values of the solution in question. (With $B_0 = B_2$ and $C_0 = C_2$ these amplitudes satisfy crossing Eqs. (12) and (13) on the mass shell. Since the symmetry point value is used in the fitting procedure, Eq. (12) remains satisfied, but Eq. (13) is forfeited to achieve the fit.) Imposing the condition $T_0^{+-} = \frac{1}{6}(2T_0^0+T_0^2) = 0$ yields the relation

$$\Delta^2 = \left(\frac{B_2-4B_0+4C_0-C_2}{8B_0+2C_0+B_2+C_2}\right)(s-1) \qquad (32)$$

which has slope (C-B)/(3B+C) when the B's and C's are equal. In Fig. 17 the slopes computed for Eq. (32) are plotted against the λ values for the solutions to which the B's and C's were fitted. For comparison, the slopes computed by linearly extrapolating the crossing symmetric amplitudes (equal B's and C's, evaluated using Eq. (14) and the relation of λ to $A_0^0(sp)$) are also shown.

Since the s intercept of Eq. (32) is known, one experimental point is sufficient to compute the slope. The 300-400 MeV point of Ref. 14 was used to compute the "experimental" value for Fig. 17, rather than a fit to points up to 600 MeV. (If the points to 600 MeV were used, the center of the "experimental" band would be raised from 1.02 to 1.3.) This was done because for all resonant solutions Re A_0^0 (which increases above threshold) peaks between 400 and 510 MeV, then decreases to zero at the resonance position.

Under linear extrapolation of symmetry point magnitudes and slopes, the solution with $\lambda = -.008$ agrees with experiment. The ratio of the scattering lengths predicted by this linear extrapolation is -3.5. (Linear extrapolation for a solution with $\lambda = -.006$, which agrees with the experimental slope of 1.3 quoted in Ref. 14, yields a ratio of -3.1 in close agreement with their result of -3.2.) However, for the solution (not the extrapolation) with $\lambda = -.008$, $a_0/a_2 = -6.4$. Clearly this ratio is extremely sensitive to the non-linearity of the solutions. The necessity of incorporating the non-linearity of the solutions when extrapolating them above threshold for comparison with experiment is obvious.

When linear amplitudes are fitted to the solutions and extrapolated as described, agreement with experiment is obtained for the solution with $\lambda = .03$, for which $a_0/a_2 \approx 0$. Thus, once again agreement with experiment is obtained for a solution in the range of λ preferred on the basis of self-consistency under the sum rule test of Section IV.

A final experimental test is provided by the value of $|\delta_0^0 - \delta_0^2|$ at 500 MeV, deduced from the charged-to-neutral decay ratio of the K_s^0. Kalmus[15] quotes a value of $40 \begin{smallmatrix} + 15^\circ \\ - 20 \end{smallmatrix}$ based on the work of the Rochester group.[16] As is seen in Table I, solutions with $\lambda \geq .020$ pass this test.

Thus agreement with experiment is obtained for solutions in the range $.007 < \lambda < .03$, which lies within the range preferred by the sum rule test of Section IV. With this impressive agreement as encouragement, the solution with $\lambda = .020$ is selected as the "best" solution. This selection is not made simply because .02 is central to the experimentally preferred

values, but rather on the basis of the low energy behavior of the experimental points of Fig. 15. The low energy peaking of the cross section ratio plotted there provides a test which is insensitive to normalization errors, and is consequently much more convincing than that of Fig. 16. It is also more convincing than the long off-mass-shell extrapolation (from $\Delta^2 = -1$ to $+6$) of the linear fitted amplitudes leading to the prediction of $\lambda = -.03$. It is extremely satisfying to be able to thus select a single solution, within the range preferred by theory, as best.

VI. SUMMARY AND CONCLUSION

It has thus been possible to produce a "best" solution to the coupled s and p-wave inverse amplitude dispersion relations for $\pi\pi$ scattering which is in agreement with all known features of the $\pi\pi$ interaction at low energies. This solution was selected from a range of solutions obtained using as input only the physical mass and width of the ρ resonance, plus the restrictive conditions of analyticity, elastic unitarity and crossing symmetry.

In order to obtain the resonant I = 0 s-wave solutions of interest it was necessary to insert (CDD) pole terms into both s-wave dispersion relations, thus allowing zeros of the amplitude between the cuts. However, it was seen that the motivation for the insertion of such poles was contained within the formalism itself, and no predictions from other formalisms were used in obtaining the solutions.

Subtraction constants and pole-term parameters for the s-waves were chosen to satisfy approximate crossing symmetry in the form of derivative conditions to third order. The importance of the third derivative condition in achieving resonant I = 0 s-waves was demonstrated by a series of calculations showing that it was well satisfied for a wide range of solutions obtained when such a resonance was imposed, and that it allowed an unambiguous choice to be made among various resonant solutions produced when the I = 2 s-wave was constrained to experimental values.

Scattering lengths were obtained in good agreement with the "universal curve" previously obtained elsewhere, and the general features of this curve were found to be explainable in terms of linear extrapolations of

symmetry point values of magnitudes and slopes of the s-wave amplitudes obtained from the lowest order crossing conditions. Nevertheless, the deviations of these amplitudes from linearity was seen to affect drastically the s-wave scattering length ratio a_0/a_2, necessitating careful investigation of recent analyses deducing experimental values for this ratio. The "best" solution was chosen as the result of these investigations, and belonged to the range of solutions preferred on the basis of a sum rule. Thus theory provides a self-consistent picture of the low energy $\pi\pi$ interaction which is able to accommodate all aspects of the experimental knowledge of this subject.

VII. ACKNOWLEDGEMENTS

It is a pleasure to acknowledge many discussions with Claude Kacser. The hospitality of the faculty and staff of the Center for Theoretical Physics, and of the Computer Science Center is greatly appreciated.

TABLE I

Scattering lengths and symmetry point values for the p-wave, and s-wave phase shift differences at 500 MeV for the resonant solutions whose phase shifts are shown in Fig. 10 (method C).

λ	$\mu^3 a_1$	$F_1(sp)$	$\lvert\delta_0^0-\delta_0^2\rvert$
.040	.0312	35.6	44°
.020	.0320	33.8	53
.007	.0327	32.6	63
-.008	.0333	31.4	70
-.020	.0337	30.7	72
-.033	.0342	30.0	77

FOOTNOTES

1. C. Lovelace, R. M. Heinz and A. Donnachie, Phys. Letters 22, 332 (1966).

2. D. Morgan and G. Shaw, Nucl. Phys. B10, 261 (1969); Phys. Rev. 10, July (1970).

3. S. Weinberg, Phys. Rev. Letters 17, 616 (1966).

4. E. P. Tryon, Proceedings of the Conference on $\pi\pi$ and $K\pi$ Interactions, Argonne National Laboratory (May, 1969).

5. G. F. Chew, S. Mandelstam and H. P. Noyes, Phys. Rev. 119, 478 (1960).

6. B. H. Bransden and J. W. Moffat, Nuovo Cimento XXI, 505 (1961).

7. K. Kang, Phys. Rev. 134, B1324 (1964).

8. Y. Fujii and K. Hayashi, Progr. Theoret. Phys. (Kyoto) 39, 126 (1968).

9. B. F. Gore, Phys. Rev. 183, 1431 (1969).

10. In evaluating the numerical integrals the integration variable was changed to $(\nu+1)^{-1/2}$ for $\nu > 0$ and $(-\nu)^{-1/2}$ for $\nu < -1$, and the unit interval of integration was divided into forty equal sub-intervals for evaluation by Simpson's rule. This grid, extremely fine near threshold and growing coarser with increasing $|\nu|$, allows a more accurate evaluation of the better known contributions near threshold. It was convenient to impose conditions at grid points, and the grid point closest to the ρ mass was at 745 MeV.

11. M. G. Olsson, U. of Wisconsin preprint COO-270 (January, 1970).

12. W. Deinet, A. Menzione, H. Müller, H. M. Staudenmaier, S. Buniatov and D. Schmitt, Phys. Letters 30B, 359 (1969).

13. D. Cline, K. J. Braun and V. R. Scherer, Proceedings of the Argonne Conference (1969).

14. L. J. Gutay, F. T. Meiere and J. H. Scharenguivel, Phys. Rev. Letters 23, 431 (1969).

15. G. E. Kalmus, Proceedings of the Argonne Conference (1969).

17. B. Gobbi, D. Green, W. Habel, R. Moffet and J. Rosen, Phys. Rev. Letters 22, 682 (1969).

FIGURE CAPTIONS

1. s-wave phase shifts, labeled by λ, for typical solutions obtained when a σ of 745 MeV was required (method A).
2. s-wave scattering lengths, with λ values indicated, obtained when a σ of 745 MeV was required (method A).
3. Right and left hand sides of Eq. (16) as a function of λ for solutions obtained when a σ of 745 MeV was required (method A). The solid curve is the left (s-wave) side and the dashed curve is the right (p-wave) side.
4. Typical s-wave phase shifts for positive λ, obtained when $\delta_0^2 = -20°$ at 745 MeV was required (method B). The solid curves show δ_0^0 and the dashed curves show δ_0^2. Since the δ_0^2 curves interpolate smoothly between bounding solutions, some have been left out for clarity. All phase shifts are modulo π.
5. Typical s-wave phase shifts, labeled by λ, obtained when $\delta_0^2 = -15°$ at 745 MeV was required (method B). Solid and dashed curves are as in Fig. 4.
6. Typical s-wave phase shifts, labeled by λ, obtained when $\delta_0^2 = -10°$ at 745 MeV was required (method B). Solid and dashed curves are as in Fig. 4.
7. Typical s-wave phase shifts for negative λ obtained when $\delta_0^2 = -20°$ at 745 MeV was required (method B). Solid and dashed curves are as in Fig. 4.
8. s-wave scattering lengths of the solutions of Figs. 4-7 (method B). Values of δ_0^2 for solutions indicated by circles, triangles and

squares are -20°, -15° and -10° respectively. The curves are from Ref. 2, a required σ of 900, 765 and 600 MeV yielding the upper, middle and lower curves respectively.

9. Right and left hand sides of Eq. (16) as a function of λ for solutions obtained when δ_0^2 was fixed at 745 MeV (method B).

10. Typical s-wave phase shifts, labeled by λ, obtained when Eq. (16) was imposed (method C).

11. The s-wave scattering lengths of the solutions of Fig. 10 (method C) are indicated by crosses, and labeled by λ values. Scattering lengths predicted by a linear extrapolation from the symmetry point of the s-wave amplitudes of these solutions are indicated by the vertical marks crossing the appropriately labeled dashed lines. These latter aspects of the figure are explained in the discussion after Eq. (27).

12. Zeros of the s-wave amplitudes of the solutions of Fig. 10 (method C) labeled by λ values. Weinberg's prediction is labeled PCAC and coincides with the solution for $\lambda = -.008$. The straight line is seen to pass through the points.

13. The s-wave scattering lengths of the solutions of Fig. 10 (method C) are indicated by crosses, and labeled by λ values. The dashed lines are the predictions of Eq. (28) when the various solutions are used in evaluating the sum rule for L. Estimates of contributions to L from above 1 BeV and of errors are from Ref. 4.

14. Theoretically predicted cross sections for the reaction $\pi^+\pi^- \to \pi^o\pi^o$ calculated from the solutions of Fig. 10 (method C), plus the unitarity bound. The experimental points are from Ref. 12.

15. Ratio of the cross sections for $\pi^+\pi^- \to \pi^o\pi^o$ and $\pi^+\pi^- \to \pi^+\pi^-$. The curves are computed from the solutions of Fig. 10 and labeled by λ. Experimental points, including symbol shapes, are from Ref. 13.

16. Ratio of the cross sections for $\pi^+\pi^- \to \pi^o\pi^o$ and $\pi^+\pi^+ \to \pi^+\pi^+$. The curves are computed from the solutions of Fig. 10 (method C) and labeled by λ. Experimental points are from Ref. 13.

17. Slope, as a function of λ, of the line relating s and Δ^2 at the zeros of the asymmetry of $\pi\pi$ scattering, when one pion has mass $-\Delta^2$. The curves are from the off-mass-shell extrapolations of the solutions of Fig. 10 (method C). The solid curve represents the extrapolations of linear amplitudes with magnitudes and slopes fitted at the symmetry point, and the dashed curve represents the extrapolations of linear amplitudes fitted to magnitudes at the symmetry point and at 400 MeV. The horizontal band represents the experimental result obtained from a modification of the analysis of Ref. 14.

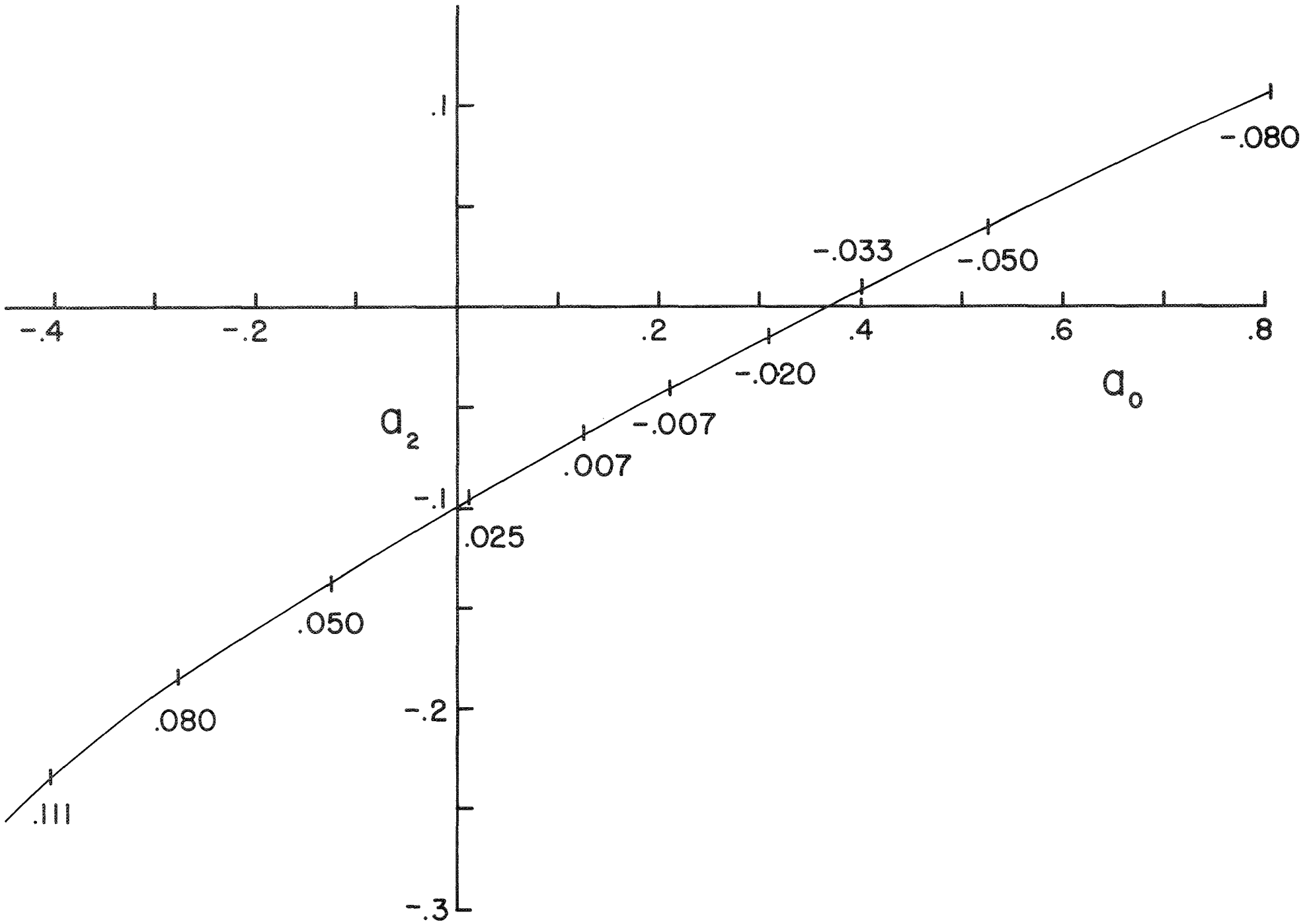
.1
-.4
-.2
.2
.4
.6
.8
-.080
-.033
-.050
-.020
-.007
.007
a_0
a_2
-.1
.025
.050
.080
-.2
.111
-.3

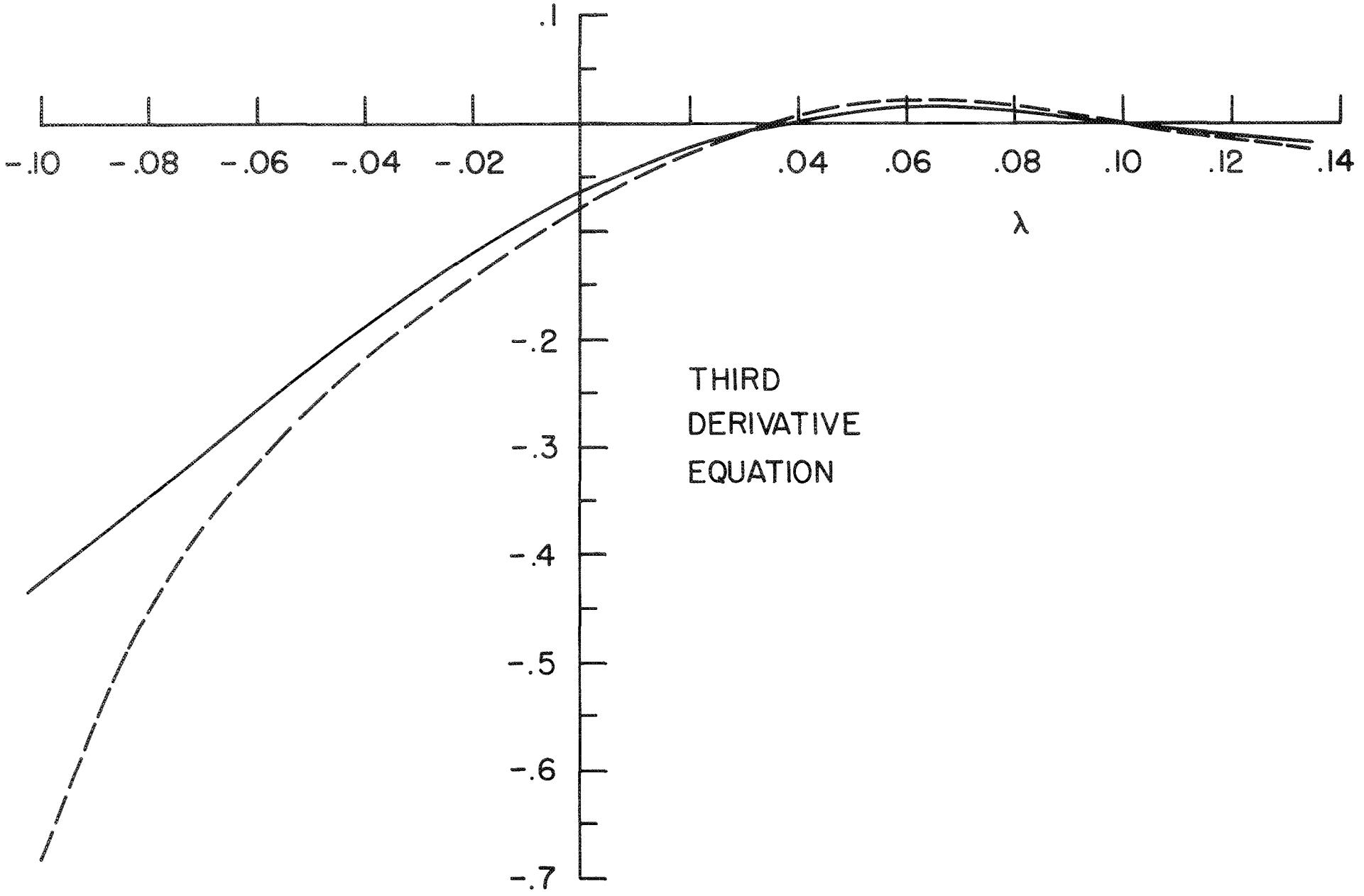
.1
-.10
-.08
-.06
-.04
-.02
.04
.06
.08
.10
.12
.14
λ
-.2
-.3
-.4
-.5
-.6
-.7
THIRD
DERIVATIVE
EQUATION

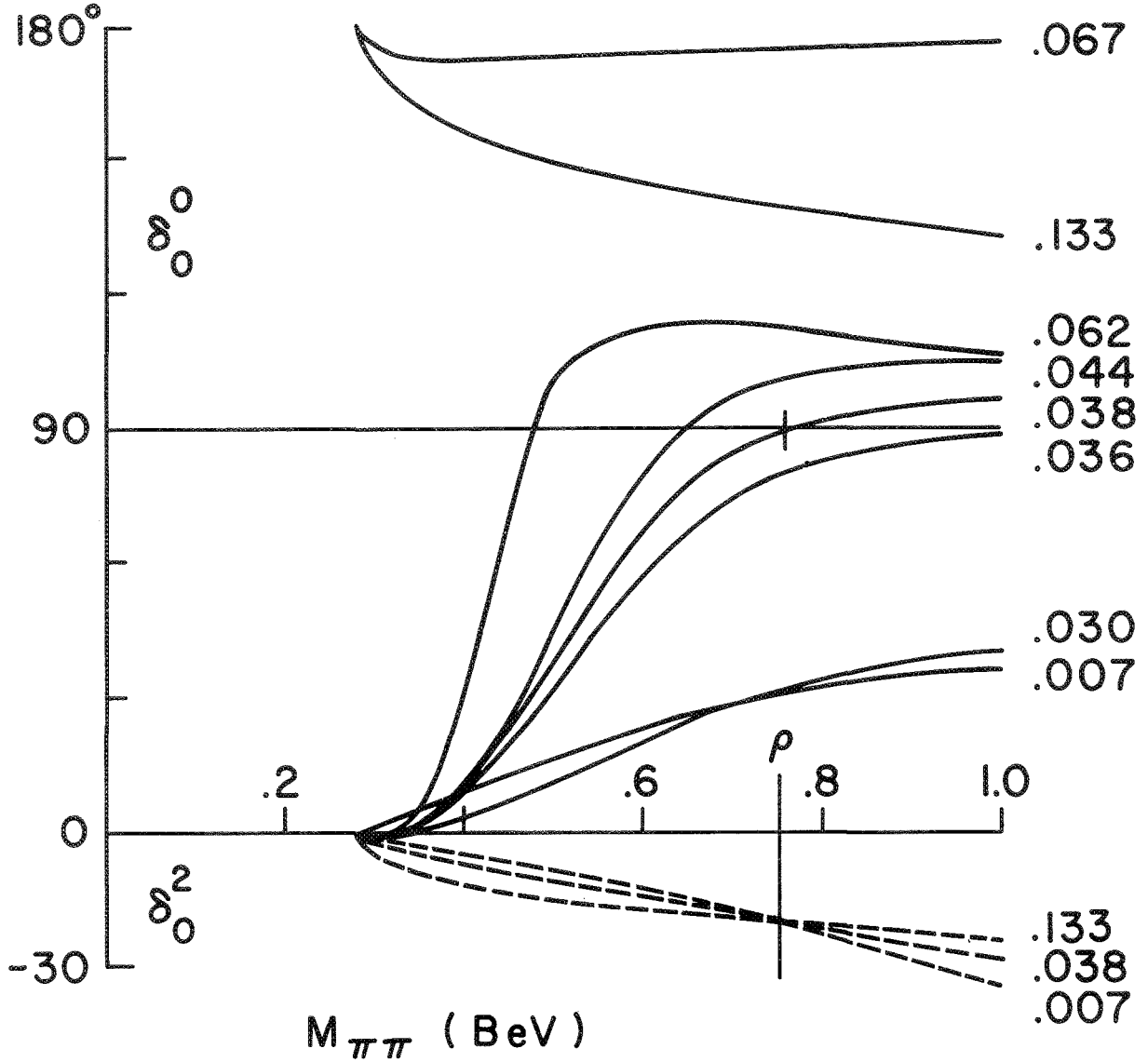
180°
90
0
-30
δ_0^0
δ_0^2
.067
.133
.062
.044
.038
.036
.030
.007
.133
.038
.007
.2
.6
.8
1.0
ρ
$M_{\pi\pi}$ (BeV)

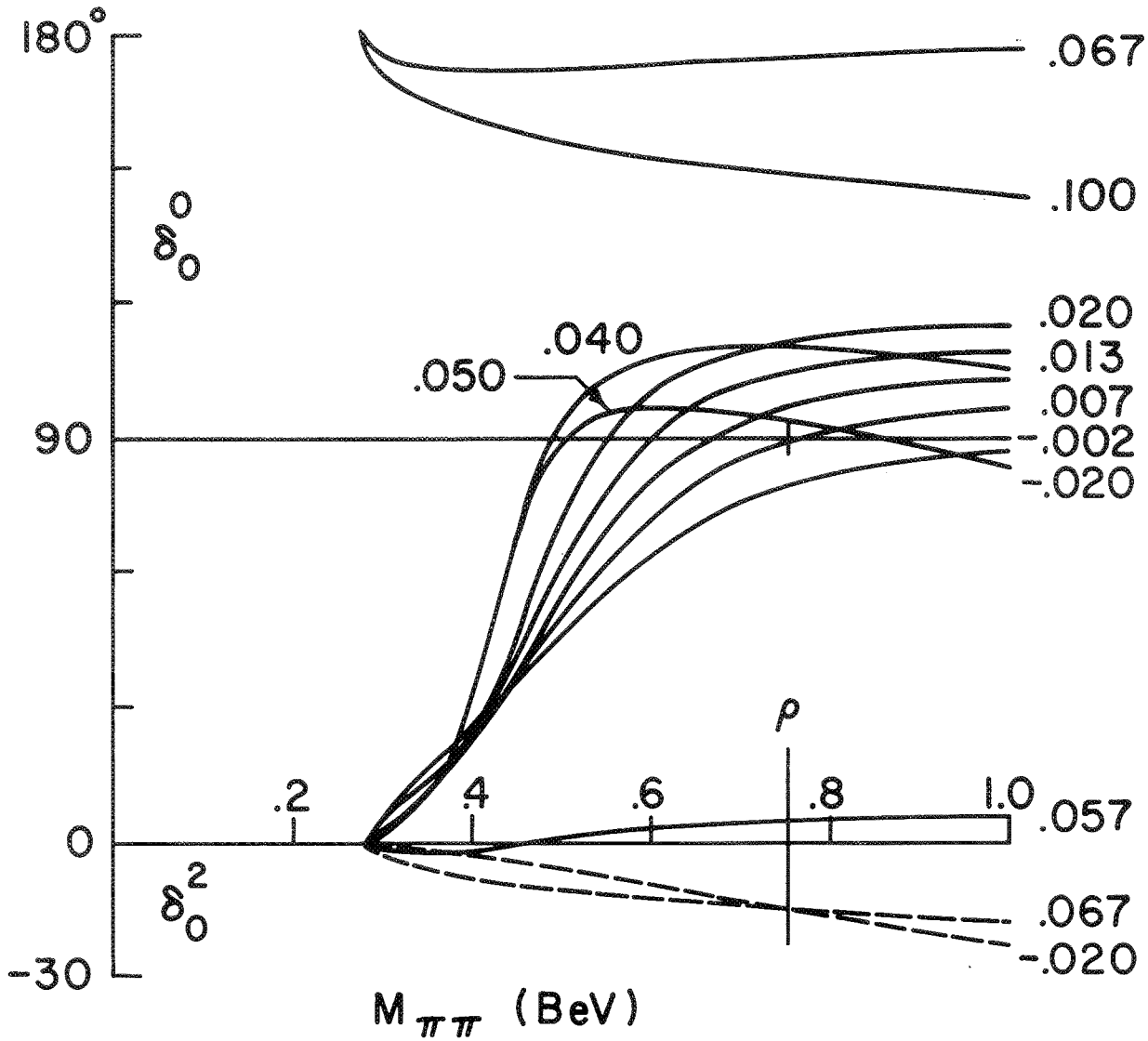
180°
90
0
-30
δ_0^0
δ_0^2
.067
.100
.020
.013
.007
-.002
-.020
.040
.050
.057
.067
-.020
ρ
.2
.4
.6
.8
1.0
$M_{\pi\pi}$ (BeV)

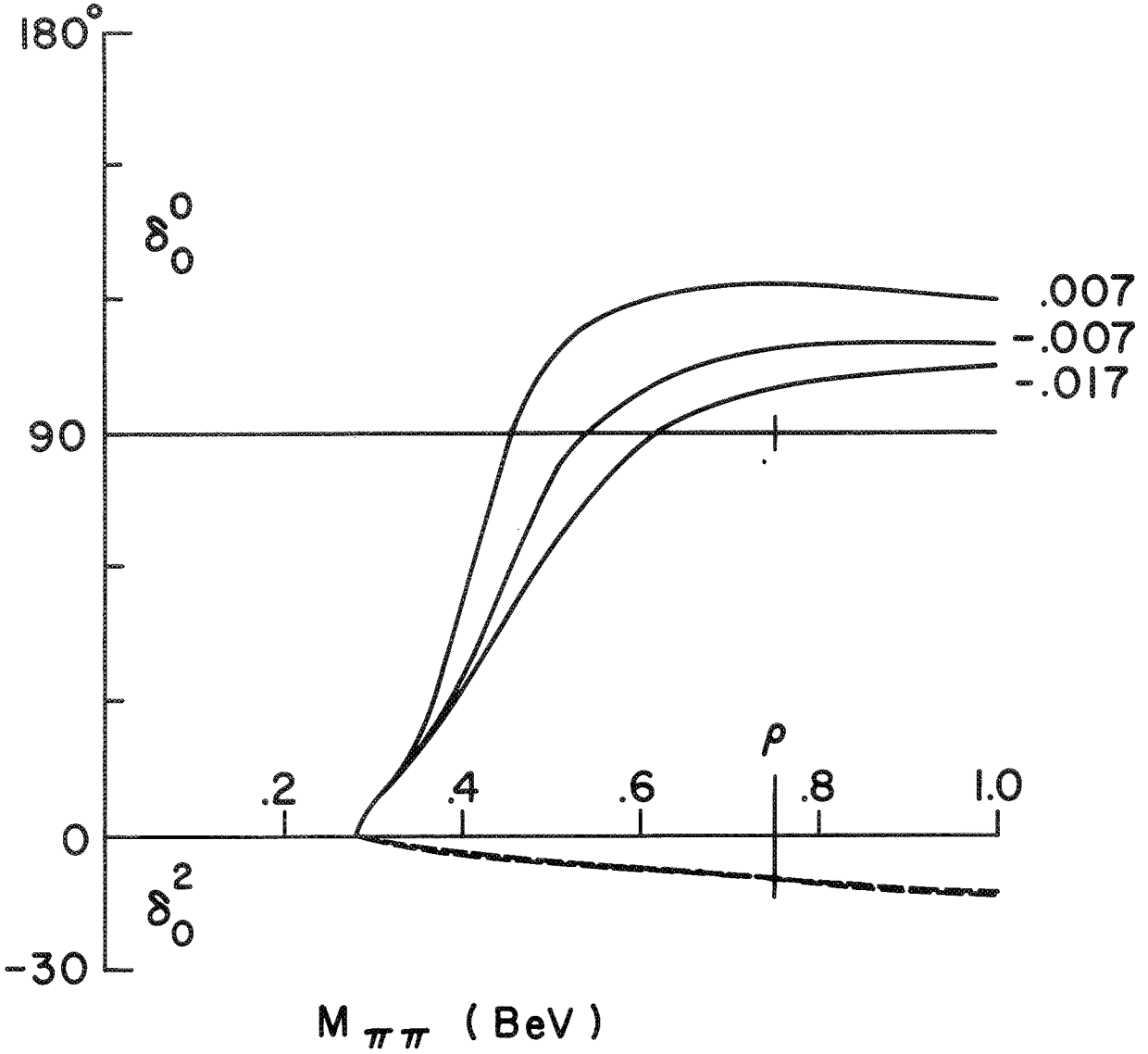
180°
90
0
-30
δ_0^0
δ_0^2
.007
-.007
-.017
ρ
.2
.4
.6
.8
1.0
$M_{\pi\pi}$ (BeV)

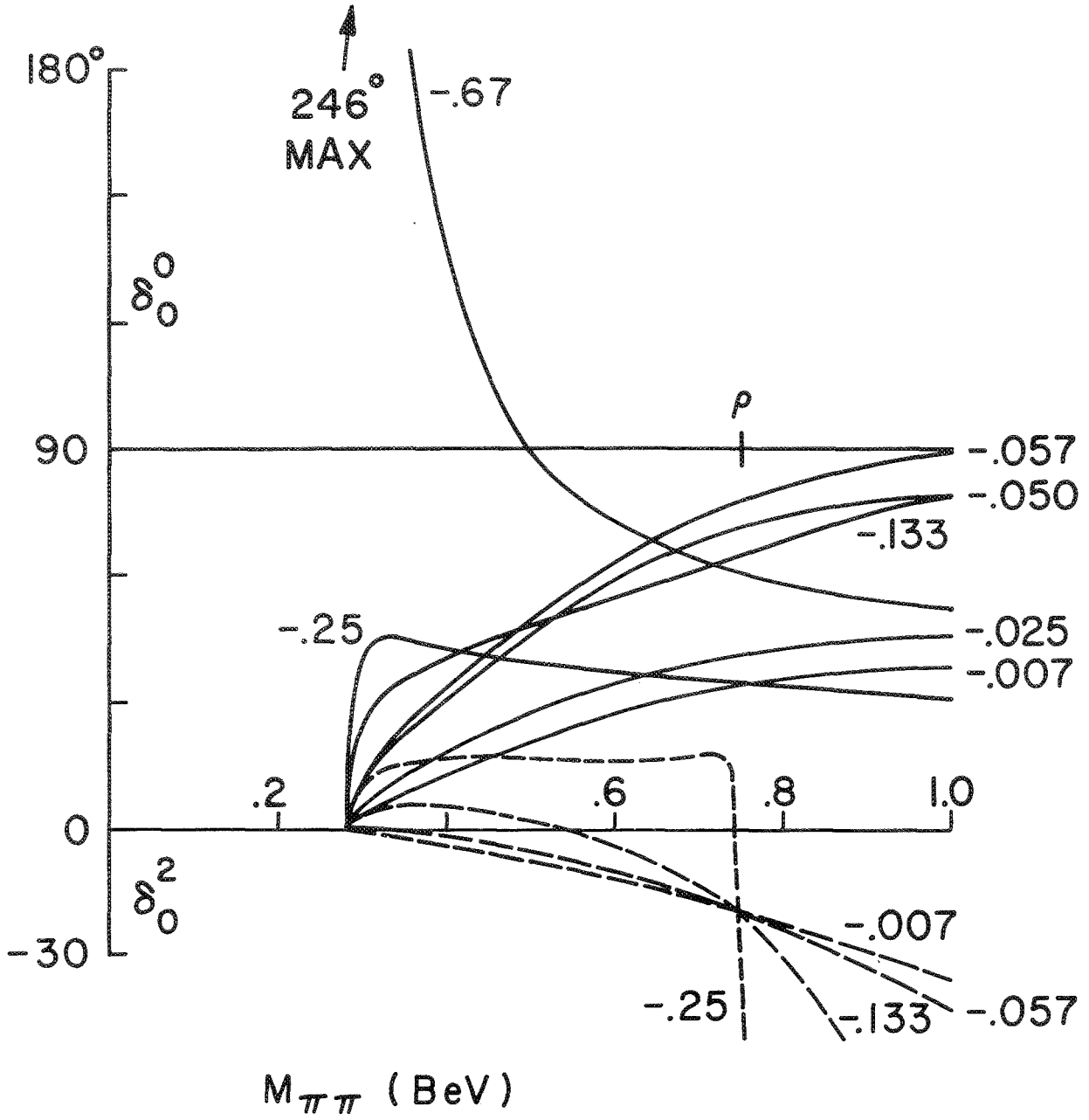
180°
246°
MAX
-.67
δ_0^0
ρ
90
-.057
-.050
-.133
-.25
-.025
-.007
.2
.6
.8
1.0
0
δ_0^2
-.007
-.30
-.25
-.133
-.057
$M_{\pi\pi}$ (BeV)

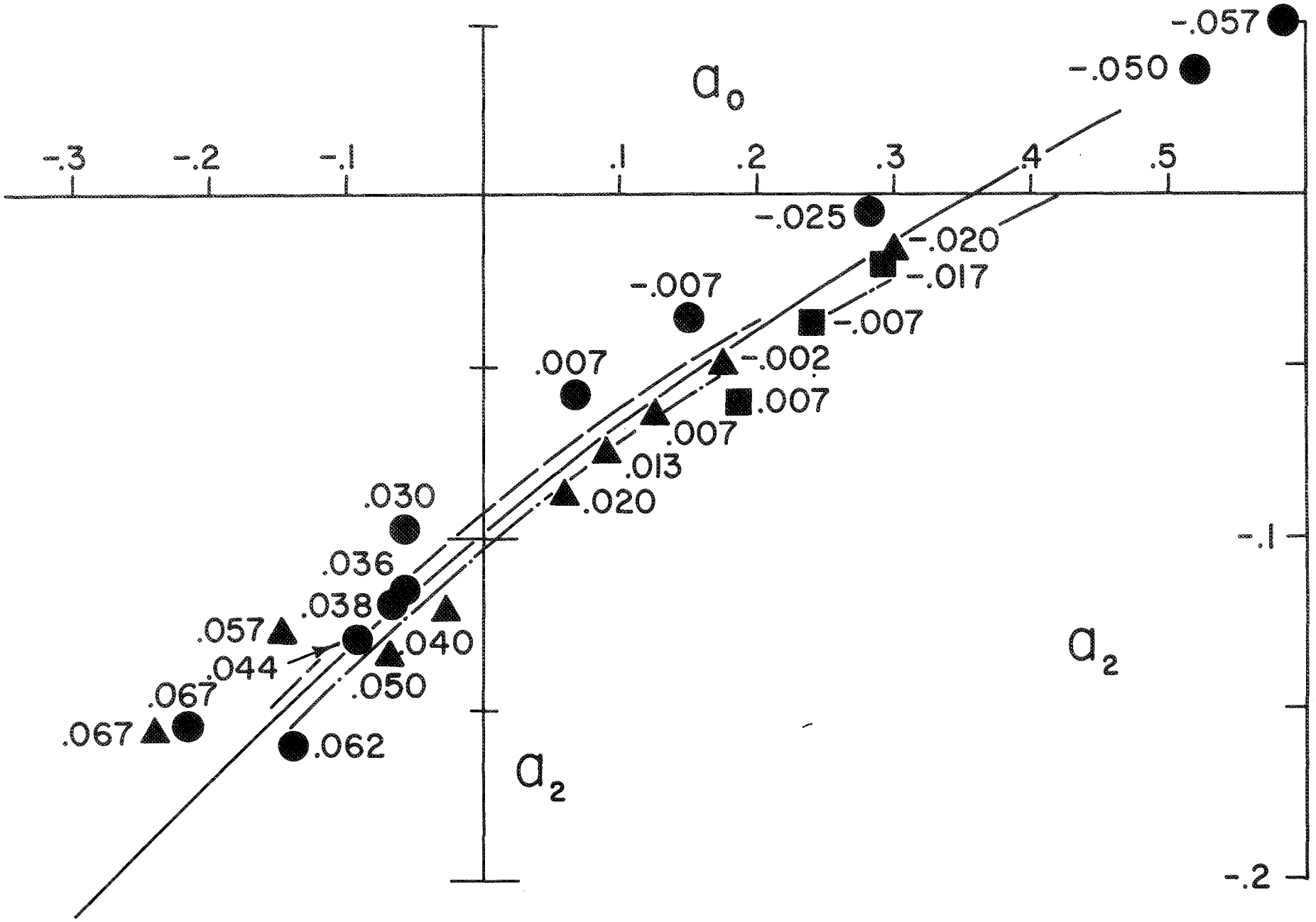
a_0
a_2
a_2
-.3
-.2
-.1
.1
.2
.3
.4
.5
-.1
-.2
-.057
-.050
-.025
-.020
-.017
-.007
-.007
-.002
.007
.007
.007
.013
.020
.030
.036
.038
.040
.044
.050
.057
.062
.067
.067

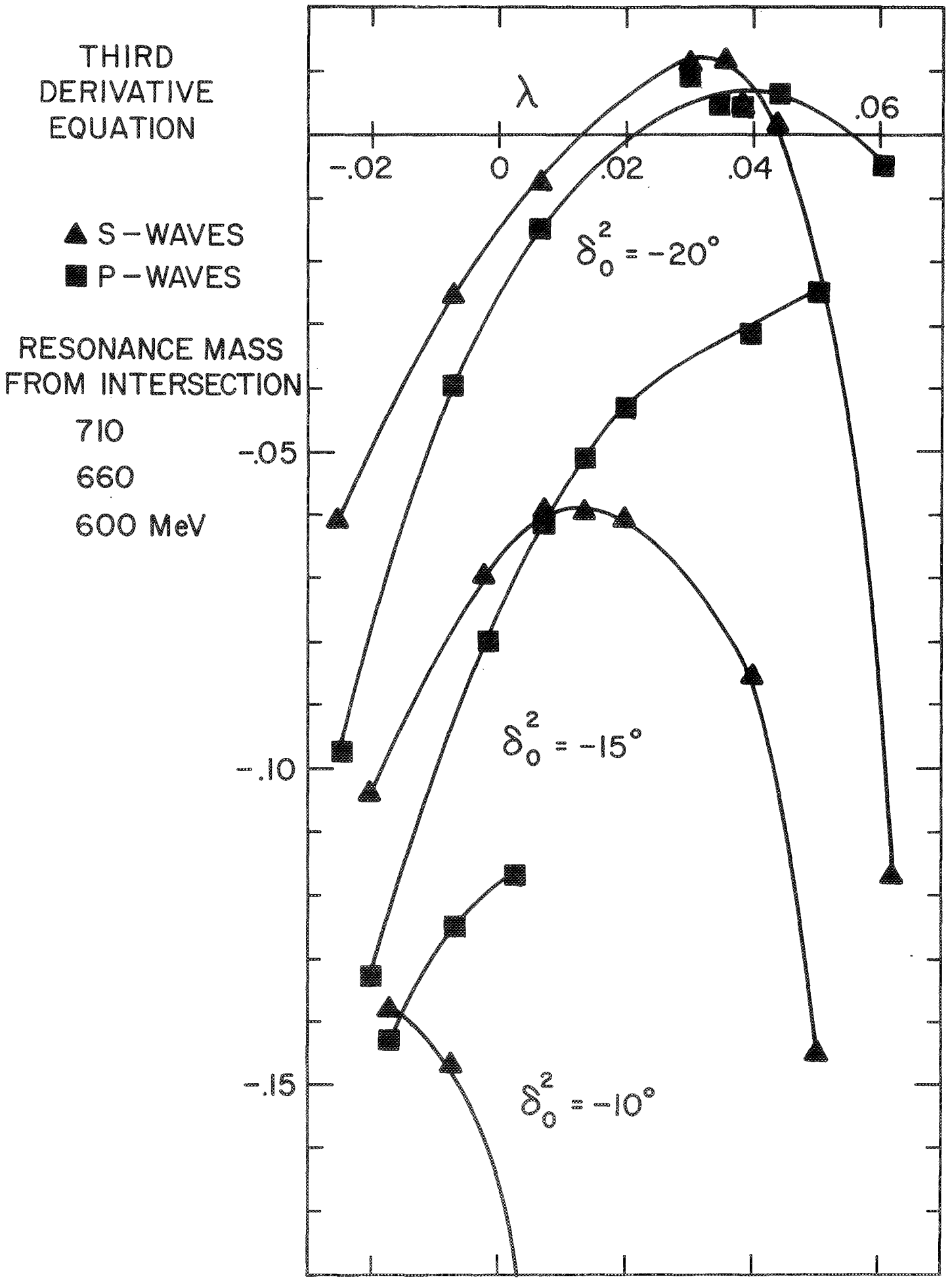
THIRD
DERIVATIVE
EQUATION
▲ S – WAVES
■ P – WAVES
RESONANCE MASS
FROM INTERSECTION
710
660
600 MeV
λ
-.02
0
.02
.04
.06
-.05
-.10
-.15
$\delta_0^2 = -20°$
$\delta_0^2 = -15°$
$\delta_0^2 = -10°$

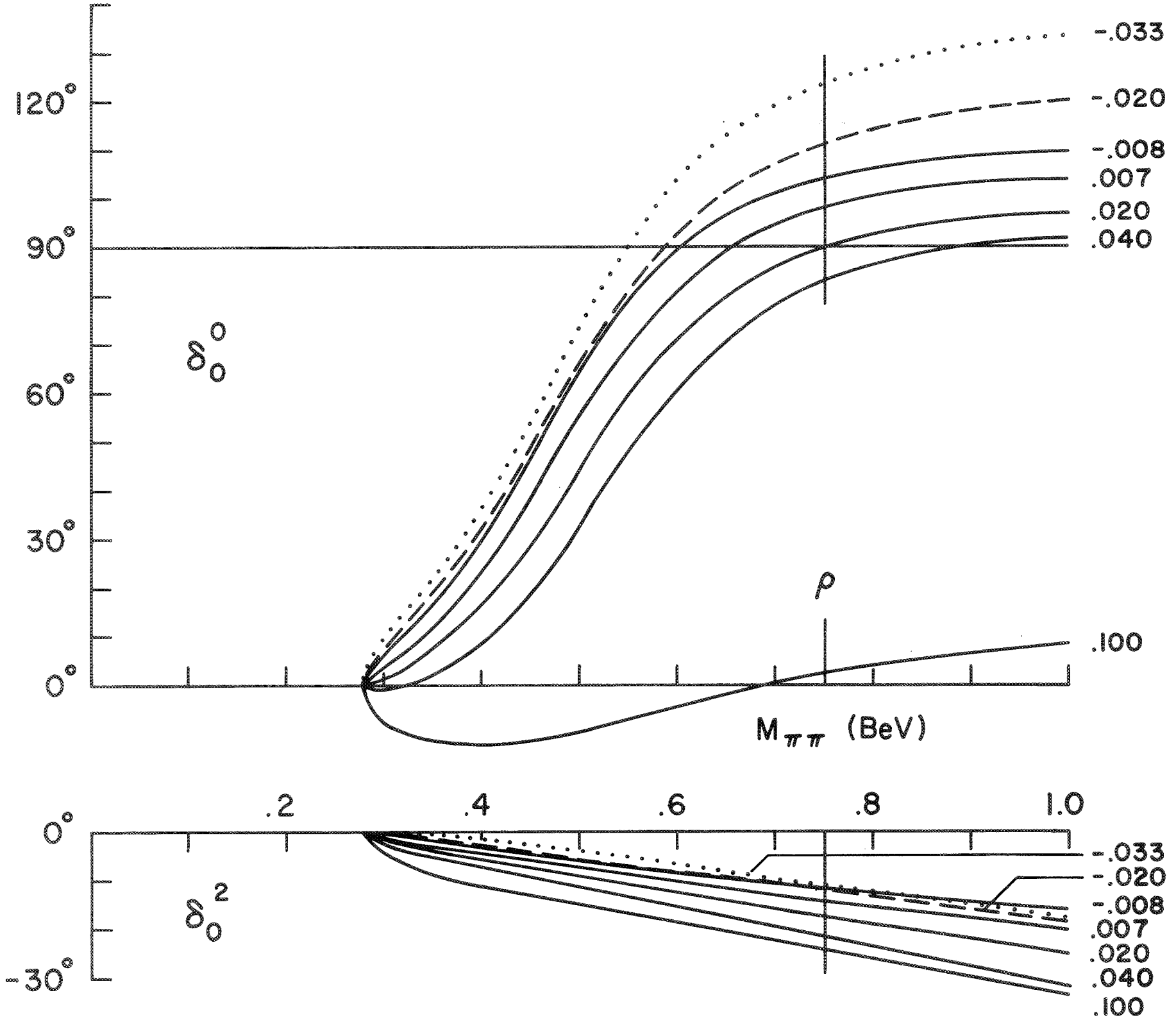
120°
90°
60°
30°
0°
δ_0^0
-.033
-.020
-.008
.007
.020
.040
ρ
.100
$M_{\pi\pi}$ (BeV)
.2
.4
.6
.8
1.0
0°
-30°
δ_0^2
-.033
-.020
-.008
.007
.020
.040
.100

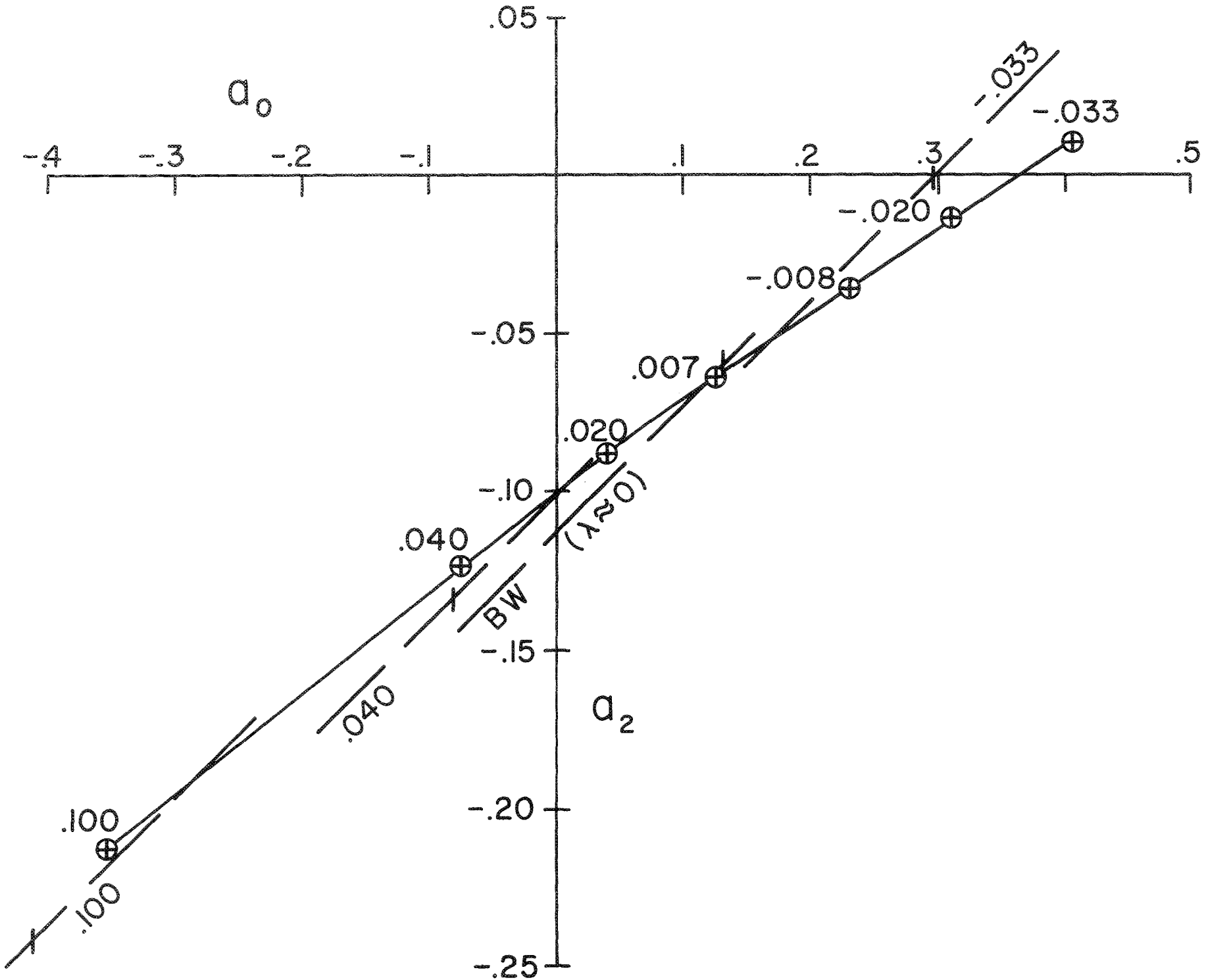
.05
a_0
-.4
-.3
-.2
-.1
.1
.2
.3
.5
-.033
-.033
-.020
-.008
-.05
.007
.020
-.10
.040
(02Y)
BW
-.15
a_2
.040
.100
.100
-.20
-.25

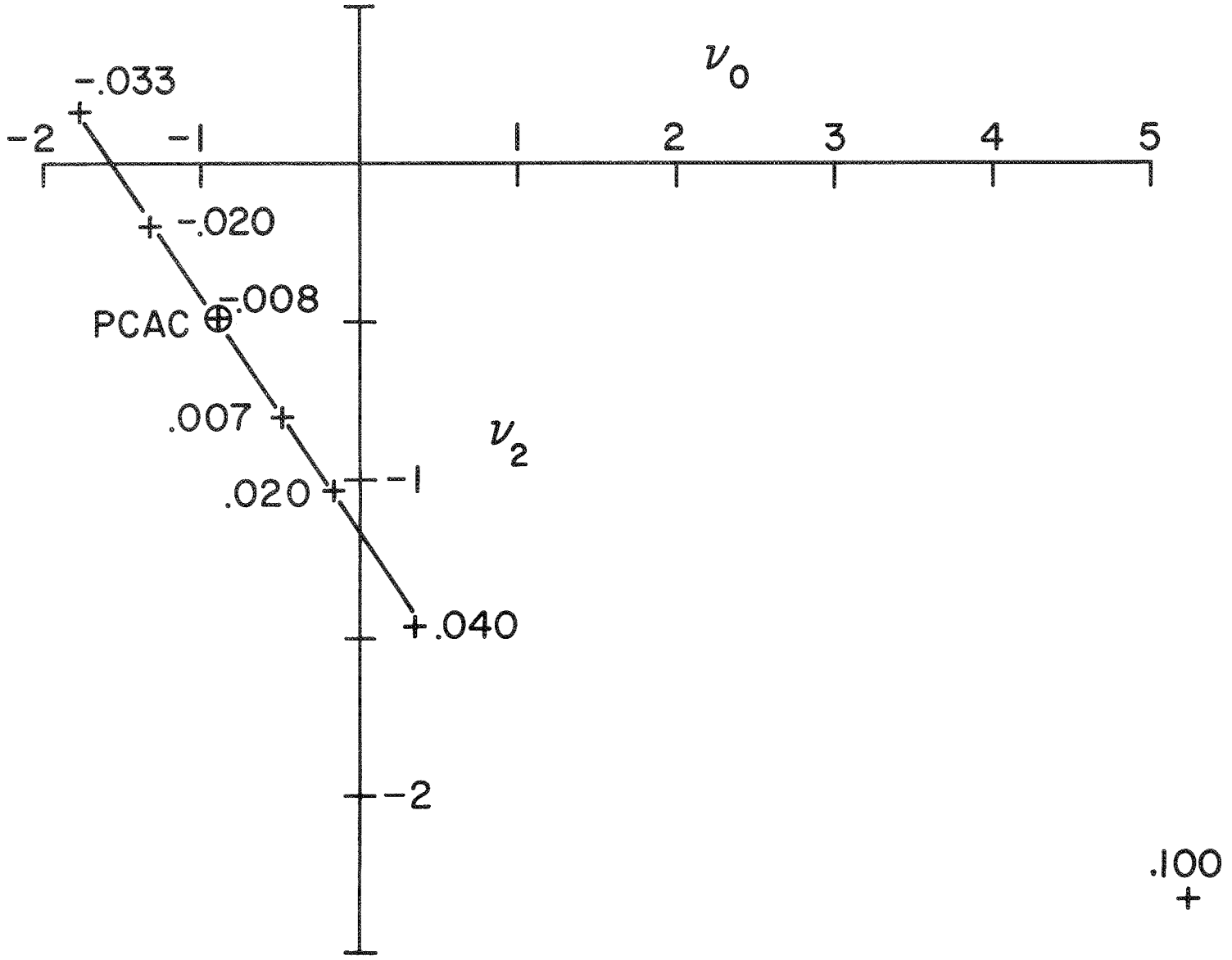
ν_0
-.033
-2
-1
1
2
3
4
5
-.020
-.008
PCAC
.007
ν_2
.020
-1
+.040
-2
.100

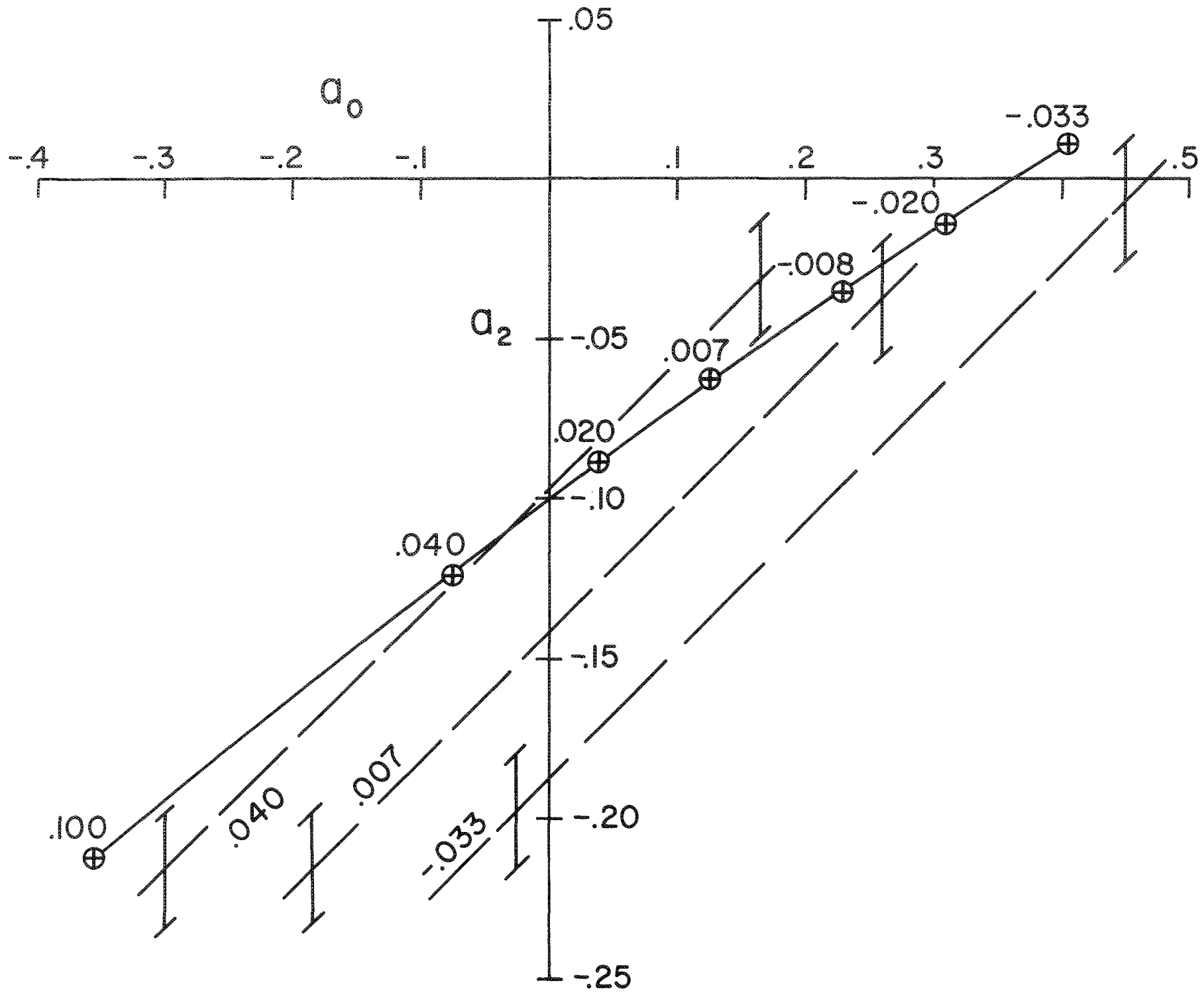
a_0
a_2
-.4
-.3
-.2
-.1
.1
.2
.3
.5
.05
-.05
-.10
-.15
-.20
-.25
-.033
-.020
-.008
.007
.020
.040
.100
.040
.007
-.033

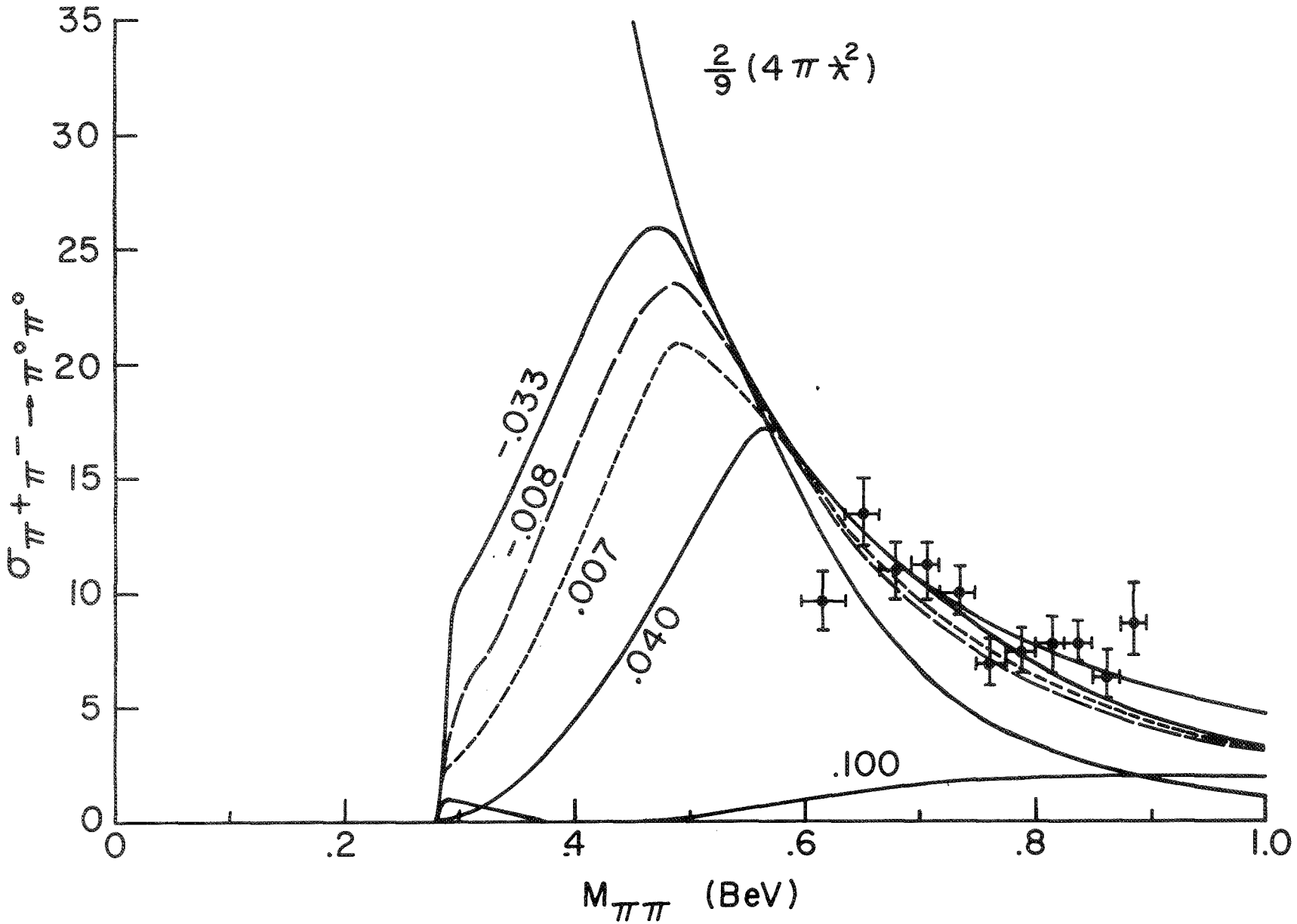
35
30
25
20
15
10
5
0
0
.2
.4
.6
.8
1.0
$\sigma_{\pi^+\pi^-\to\pi^0\pi^0}$
$M_{\pi\pi}$ (BeV)
$\frac{2}{9}(4\pi\lambda^2)$
-.033
-.008
.007
.040
.100

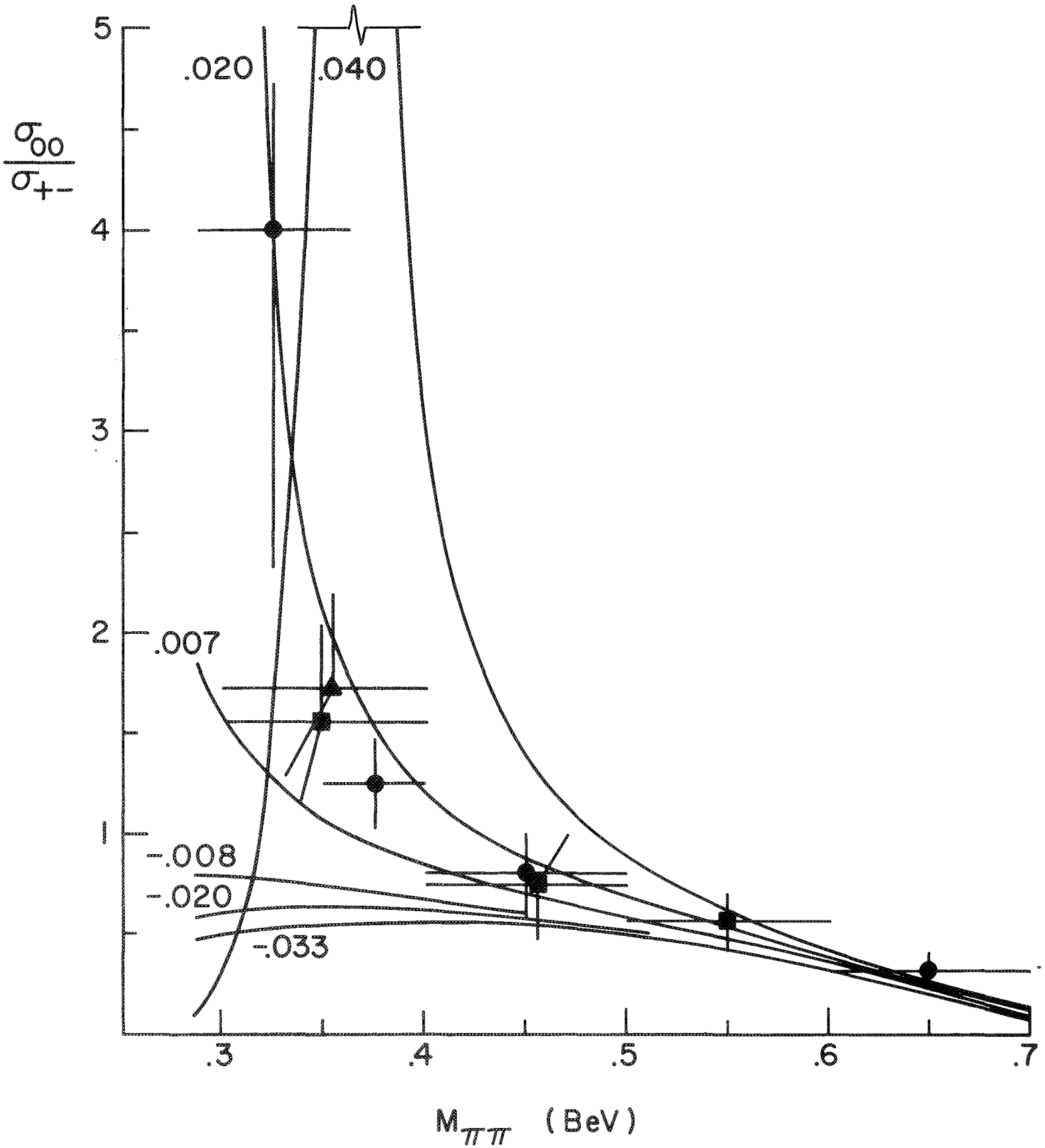
5
4
3
2
1
$\frac{\sigma_{00}}{\sigma_{+-}}$
.020
.040
.007
-.008
-.020
-.033
.3
.4
.5
.6
.7
$M_{\pi\pi}$ (BeV)

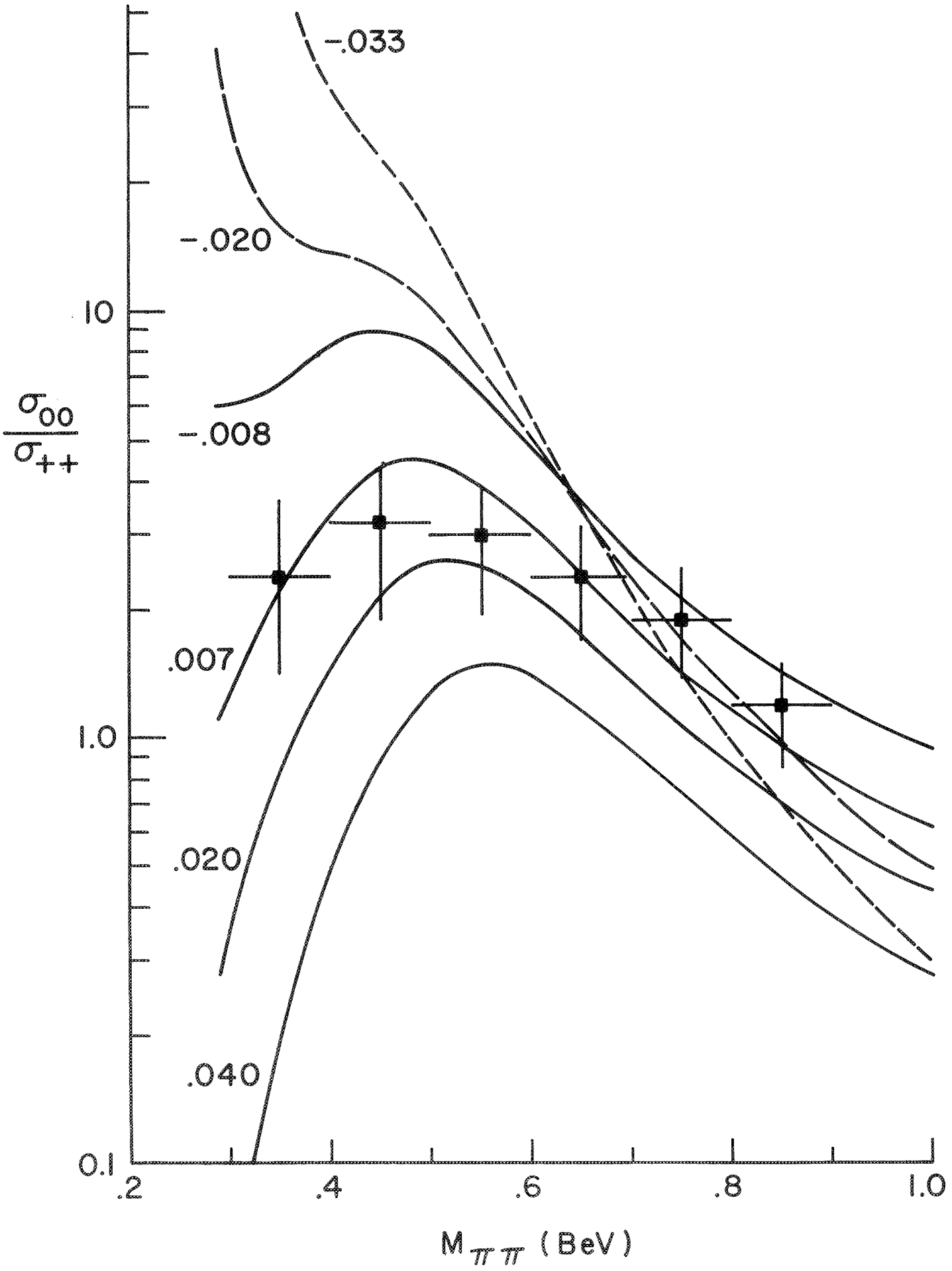
-.033
-.020
-.008
.007
.020
.040
10
1.0
0.1
$\frac{\sigma_{00}}{\sigma_{++}}$
.2
.4
.6
.8
1.0
$M_{\pi\pi}$ (BeV)

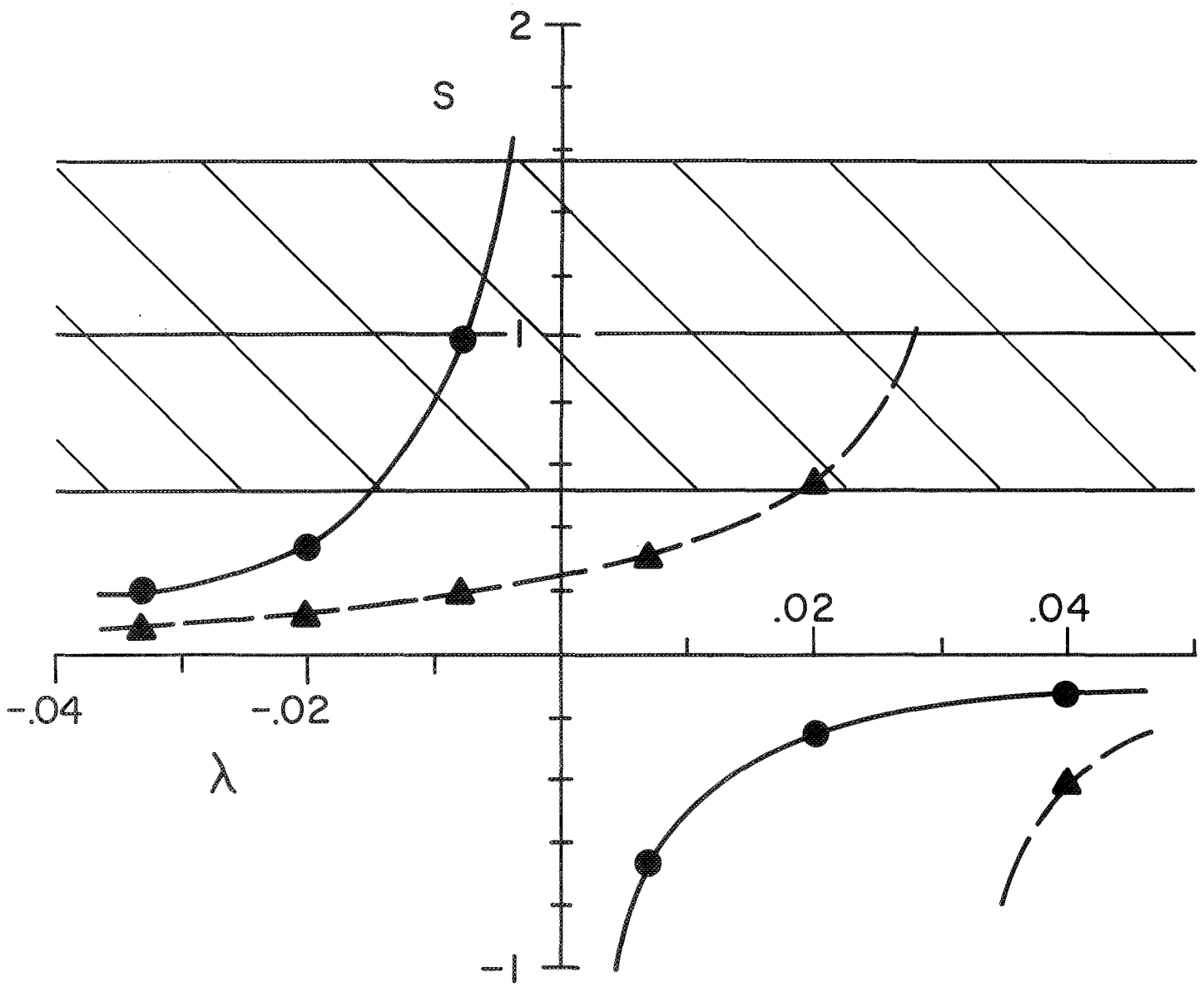
2
S
1
.02
.04
-.04
-.02
λ
-1